Abnormal behavior in a chromosome-engineered mouse model for human 15q11-13 duplication seen in autism

Jin Nakatani[1,10], Kota Tamada[1,2,10], Fumiyuki Hatanaka[1,3], Satoko Ise[4], Hisashi Ohta[4], Kiyoshi Inoue[1], Shozo Tomonaga[1], Yasuhito Watanabe[1,2], Yeun Jun Chung[5], Ruby Banerjee[5], Kazuya Iwamoto[6], Tadafumi Kato[6,7], Makoto Okazawa[1], Kenta Yamauchi[8], Koichi Tanda[8], Keizo Takao[8,9], Tsuyoshi Miyakawa[8,9], Allan Bradley[5] & Toru Takumi[1,3,7]

[1]Osaka Bioscience Institute, Suita, Osaka 565-0874, Japan

[2]Kyoto University Graduate School of Biostudies, [3]Department of Molecular Neuroscience, [8]Frontier Technology Center, Kyoto University Graduate School of Medicine, Sakyo, Kyoto 606-8501, Japan

[4]Tsukuba Research Institute, Banyu Pharmaceutical Co. Ltd., Tsukuba, Ibaraki 300-2611, Japan

[5]The Wellcome Trust Sanger Institute, Hinxton, Cambridge CB10 1SA, UK

[6]Brain Science Institute, RIKEN, Wako, Saitama 351-0198, Japan

[7]Graduate School of Biomedical Sciences, Hiroshima University, Minami, Hiroshima 734-8553, Japan

[9]Division of Systems Medicine, Institute for Comprehensive Medical Science, Fujita Health University, Toyoake, Aichi 470-1192, Japan

[10]These authors contributed equally to this study.

To whom correspondence should be addressed: Toru Takumi (e-mail:takumi@hiroshima-u.ac.jp), Laboratory of Integrative Bioscience, Graduate School of Biomedical Sciences, Hiroshima University, 1-2-3 Kasumi, Minami, Hiroshima 734-8553, Japan, Tel: +81-82-257-5115, Fax: +81-82-257-5119

Autism is a complex psychiatric illness that has received considerable attention as a developmental brain disorder. Substantial evidence suggests that chromosomal abnormalities contribute to the risk of autism. The duplication of human chromosome 15q11-13 is known to be the most frequent cytogenetic abnormality in autism. We have modeled this genetic change in mice using chromosome engineering to generate a 6.3-Mb duplication of the conserved linkage group on mouse chromosome 7. Mice with a paternal duplication display autistic behavioral features such as poor social interaction, behavioral inflexibility, abnormal ultrasonic vocalizations, and correlates of anxiety. An increased MBII52 snoRNA within the duplicated region, affecting the serotonin 2c receptor (5-HT2cR), correlates with altered intracellular Ca^{2+} responses elicited by a 5-HT2cR agonist in the neurons in mice with a paternal duplication. This first chromosome-engineered mouse model for autism replicates various aspects of human autistic phenotypes and validates the relevance of the human chromosome abnormality. This model will facilitate forward genetics of developmental brain disorders and serve as an invaluable tool for therapeutic development.

Introduction

Autism is a common and heterogeneous neuropsychiatric disorder with manifestations of deficit in social interaction, impaired communication and repetitive behavior or restricted interest (Volkmar and Pauls, 2003). Its definition has been extended to autism spectrum disorder (ASD) including autism-related disorders such as Asperger disorder and Rett's syndrome (DiCicco-Bloom et al., 2006; Geschwind and Levitt, 2007; Lord et al., 2000; Veenstra-VanderWeele et al., 2004). Autism is now considered as a developmental brain disease (Belmonte et al., 2004; DiCicco-Bloom et al., 2006; Dykens et al., 2004; Geschwind and Levitt, 2007; Maestrini et al., 2000; Veenstra-VanderWeele and Cook, 2004; Vorstman et al., 2006). The first signs of autism appear at around 6 months, full diagnosis is usually made at 3 years and symptoms usually persist throughout life. Autism is one of the most heritable neuropsychiatric disorders (Geschwind and Levitt, 2007), suggesting that genetic factors play an important role in its etiology (Vorstman et al., 2006). Candidate chromosomal regions and specific genes have been investigated (Belmonte et al., 2004; Folstein and Rosen-Sheidley, 2001; Persico and Bourgeron, 2006; Polleux and Lauder, 2004). There

are likely to be de novo mutations, chromosomal abnormalities and common genetic variants that contribute to the genetic etiologies of autism (Abrahams and Geschwind, 2008; Geschwind, 2008; Geschwind and Levitt, 2007; Ramocki and Zoghbi, 2008). Several knockout mice have also been reported as "putative" autistic models, as judged from their phenotypes; but the molecular mechanism responsible for the pathophysiology of autism is far from complete.

Abnormalities of chromosomes are thought to account for 10 to 20% of autism cases (Beaudet, 2007). A recent study has established de novo germline mutations including copy number variants (CNVs) as a more significant risk factor for ASD than previously recognized (Sebat et al., 2007). Paternally or maternally inherited deletions of human chromosome 15q11-13 occur quite frequently, when they affect the imprinted region this is recognized as Prader-Willi syndrome or Angelman syndrome, respectively (Nicholls and Knepper, 2001). Duplication of the same region is the only recurrent cytogenetic aberration associated with autism, occurring in up to 5% of autism cases (Belmonte et al., 2004; Bolton et al., 2004; Cook and Scherer, 2008; Dykens et al., 2004; Folstein and Rosen-Sheidley, 2001; Lord et al., 2000; Maestrini et al., 2000;

Veenstra-VanderWeele et al., 2004; Veenstra-VanderWeele and Cook, 2004; Vorstman et al., 2006).

Based on conserved human/mouse linkage, we have generated mice with a 6.3-Mb duplication of mouse chromosome 7 mirroring the human chromosome 15q11-13 duplication. This mouse model displays several phenotypes that recapitulate aspects of the human condition and provides mechanistic insight into the disease.

Results

Construction of a 6.3-Mb duplication on mouse Chr. 7

Human chromosome 15q11-13 has a conserved linkage group on mouse chromosome 7 (Figure 1). Chromosomal engineering (Bradley and van der Weyden, 2005) was used to construct an interstitial duplication of mouse chromosome 7 corresponding to the region between common breakpoints in human chromosome 15q11-13. Sequential rounds of insertional gene targeting were used to insert the selection cassettes and *loxP* sites required for chromosome engineering proximal to the *Herc2* and distal to *Mkrn3* (Figures 1 and 2A). A double targeted clone in which the targeting had occurred on the homologous chromosomes (*trans*) was transiently transfected with a Cre expression plasmid to induce recombination between the *loxP* sites which generated clones with a balanced duplication (*Dp*) and deletion (*Df*) (Figure 2C). Recombinants were recovered by hypoxanthine-aminopterin-thymidine (HAT) selection at a frequency of 26 X 10^{-7} per electroporated cell and confirmed using Southern blot analysis (Figures 2B and 2D) and fluorescence *in situ* hybridization (FISH) (Figure 2E). The deletion and duplication alleles were transmitted and established in the germ line using standard procedures and

the expected increase in genomic copy number of this region was confirmed using comparative genomic hybridization (CGH) on a mouse Bacterial Artificial Chromosome (BAC) microarray (Figure 2F).

Increased gene expression of duplicated genes

The duplication allele was transmitted at normal Mendelian ratios from both females and males. Mice with a maternally (*matDp/+*) and paternally (*patDp/+*) inherited duplication bred normally and were fertile. The *patDp/+* male mice began to show an increase in body weight compared to wild type (WT) mice after 15 weeks and the body weight of *patDp/+* was significantly greater than that of the WT after 20 weeks (data not shown).

We performed histological analyses of the adult brain as well as that of brains at postnatal day (P) P0, P7, and P14 to screen for morphological changes. No significant abnormality was detected in HE-stained sections of the olfactory bulb, cerebral cortex, hippocampus, amygdala, corpus callosum, and cerebellum either macroscopically or at the microscopic level (Figure S1). The number of Purkinje cells in the cerebellum was

not significantly different between mice with the duplication and WT mice (Figure S2). Bodian staining was also performed and this did not reveal any significant abnormality in the cortex, hippocampus, amygdala, and cerebellum (data not shown).

The 6.3-Mb duplication includes the region of genomic imprinting. The relative expression levels of genes in the duplicated region are expected to vary depending on whether they are imprinted and on their mode of inheritance (Figure 3A). Therefore gene expression was assessed by quantitative RT-PCR in the brains from *patDp/+* and *matDp/+* mice and the results were normalized to those in WT mice (Figure 3B). In the adult brain, *Ndn*, *Snrpn*, *Ube3a*, *Gabrβ3*, *Gabrα5*, and *Herc2* genes in the duplicated region were highly expressed; whereas the expression of others was relatively less abundant. The mRNA levels of the paternally expressed genes, *Ndn*, and *Snrpn*, were increased more than 2-fold in the *patDp/+* mice. Unexpectedly, *Ndn* also exhibited increased expression levels in *matDp/+*, though the levels were lower, while *Snrpn* showed the expected level (no change). The maternally expressed gene, *Ube3a*, showed an approximately 2-fold increase in *matDp/+* mice. The expression of *Atp10a* did not show any significant difference between *patDp/+* and *matDp/+* mice. The

non-imprinting genes, $GABA_A$ receptor subunits and *Herc2*, showed the expected 1.5-fold increase in mice with the duplication. *Chrna7* and *Tubgcp5*, both of which are located outside the duplicated region, did not show any significant change in their expression levels. In other tissues, the expression phenotypes reflected those in the brain (Figure S3). The expression of each gene in various areas of the adult mouse brains was examined by *in situ* hybridization (Figure 3C). Alterations in the expression patterns of these genes in *patDp*/+ and *matDp*/+ brains were unremarkable, although the expression level of *Snrpn* in the hippocampus seemed to be higher in the *patDp*/+ mice whereas that of *Ube3a* seemed to be higher in the *matDp*/+ mice.

DNA methylation is an epigenetic modification in imprinted regions and is found in 15q11-13 (Nicholls and Knepper, 2001). The imprinting center (IC) is localized to the 5'-end of *Snurf-Snrpn* locus. This region is methylated (Me) or unmethylated (UnMe) in maternal and paternal alleles, respectively. We thus examined allele-specific methylation by Southern blotting with a *Snurf* probe using methylation sensitive (*Bss*HII) and insensitive (*Hpa*I) restriction enzymes. The ratios of Me and UnMe bands were 1:2 and 2:1 in *patDp*/+ and *matDp*/+ mice, respectively, in contrast

to 1:1 in WT (Figure 3D). These results suggest that allele-specific methylation is conserved in the mice with the duplicated allele.

patDp/+ mice display social abnormalities

To analyze the effect of the chromosomal duplication on behavior, we performed a comprehensive battery of behavioral tests (Crawley, 2007; Takao et al., 2007; Yamasaki et al., 2008). We observed significant differences between WT and mice with a duplication in the several tests described below (Table S1 and S2). The diagnosis of autism is based on behavioral criteria (Volkmar and Pauls, 2003). Therefore, a valid mouse model should reflect behavioral symptoms, including impairment in social interaction (Crawley, 2004; Moy et al., 2006).

A 3-chamber social interaction test (Crawley, 2004; Nadler et al., 2004) was performed (Figure 4A). The mouse to be tested is placed in the central chamber and can move freely among the 3 chambers. A stranger mouse is placed in one of the side chambers in a wire cage, and only a cage is placed in the opposite chamber. WT mice tended to contact the stranger mouse and the time spent with the stranger mouse in the

quadrant location depicted by the line in Figure 4A was significantly higher than the time spent in the corresponding location in the opposite chamber with the empty cage (Figure 4B). In contrast, the *patDp/+* mice exhibited no significant difference in time spent between the quadrant spaces of either side (Figure 4B). These phenotypes were also observed in mice with a different background under similar experimental conditions (Figure S4). To confirm that these results are due to specific changes in social behavior, we further performed the 3-chamber test under different conditions. First, we assessed the reaction of mice to a novel inanimate object. Both *patDp/+* and WT mice spent more time around the cage with a novel inanimate object compared with the empty cage and no significant difference between *patDp/+* and WT mice was observed (Figures 4C and S5A). Second, the simultaneous interactions with a novel mouse and another novel object were compared. WT mice spent more time around the cage with a novel mouse compared with a novel object, whereas *patDp/+* mice showed no significant difference in time spent around the cages with a novel mouse and object (Figure 4D and S5B). Third, the interactions of the mice with a novel and familiar mouse were also compared. In WT mice, although the time spent around the cages was

not significantly altered, the number of entries around the novel mouse tended to be greater than that of the familiar mouse (p=0.0541), whereas in *patDp/+* mice no significant difference between the novel and familiar mouse was found (Figure 4E and S5C). These results suggest that WT mice are more interested in a novel mouse than a novel inanimate object, but *patDp/+* mice have decreased sociability compared with WT, which may be analogous to the impairment in appropriate social interaction often seen in autistic patients (Crawley, 2004). On the other hand, *matDp/+* mice were indistinguishable from WT mice (Figure S6). Since social behavior in mice is to a large extent olfactory driven, we examined the olfactory system of the mice anatomically (by immunohistochemistry) and functionally (by olfactory habituation/dishabituation test), and excluded any defects of the olfactory system in *patDp/+* mice (data not shown).

To measure behavioral flexibility, we habitually trained mice and then analyzed their responses to a change in routine in a reversal task by using the Morris water maze test and the Barnes maze test, which have been generally validated for spatial learning and memory (Crawley, 2007; Miyakawa et al., 2001). The Morris water maze is a spatial navigation task in which the mouse swims to find a hidden platform.

Mice were trained to locate the correct platform to escape from the water. Both *patDp/+* and WT mice learned the target quadrant (TA in Figure 5A, Figures 5B and 5C), suggesting no impairment in spatial learning in *patDp/+* mice. When the target platform was then moved to the opposite area (TA in Figure 5D), WT mice spent significantly more time in the new TA quadrant compared with the opposite quadrant (OP) (Figure 5E). On the other hand, *patDp/+* mice exhibited no difference between time in the TA and OP (Figure 5F).

The Barnes maze is a circular white platform with 12 holes (Figures 5G and 5J). One of the holes exits into a dark box called the target initially placed at 0 degrees (Figure 5G). Mice were trained to locate the correct hole to exit into the escape box. Both *patDp/+* and WT mice learned to identify the target at the 0 degrees point, and there was no observable difference between the two mice (Figures 5H and 5I), again suggesting no impairment in spatial learning of *patDp/+* mice. When the target was moved to the opposite side (Figure 5J), both *patDp/+* and WT mice could find the target; however, compared with WT, *patDp/+* mice stayed less in the new target position and more in the 180 or +/-150 degrees position, which is the position of the

original target or in its direction (Figure 5L). The time spent between the target and the 180 degrees position was significantly different in WT mice (Figure 5K), whereas there was no significant difference in *patDp/+* mice (Figure 5L). The Barnes maze test was also performed in mice with a different background, and the results were consistent (Figures S7A and S7B). Conversely, *matDp/+* mice did not show any significant change even in reversal learning compared with WT mice (Figures S8A and S8B). These results suggest that *patDp/+* mice do not respond as flexibly as WT and *matDp/+* mice to a change in situation, which may be comparable to the inflexibility in routine that is characteristic of autism (Crawley, 2004), although we should acknowledge that it is far from clear how cognitive deficits in reversal learning are related to the behavioral deficits in autism even in humans and even less clear from mouse to humans (Geurts et al., 2009). Furthermore, we found the lack of reversal deficits in the T-maze test (data not shown). Perhaps reversal deficits are only apparent during aversively motivated escape behaviors and not appetitively motivated approach behaviors.

To see impairment in communicative behavior, we measured ultrasonic vocalizations (USVs) of neonatal mice that were separated from their dams (Figure 4F).

These USVs are thought to be distress signals (Crawley, 2007) and may be related to communication between a dam and her pups (Crawley, 2004). In WT mice the USVs have a normal developmental course, emerging soon after birth, peaking at around P5, and then decreasing to almost zero at around P14, the time of eye opening when the development of alternative communication may occur (Noirot, 1966). The USVs emitted by *patDp/+* pups at P7 and P14 were markedly greater than those of the WT pups (Figure 4F). In the *patDp/+* pups, the peak in the numbers of USVs seemed to be delayed and the USVs were still present at P14 when those of WT mice had disappeared, suggesting that *patDp*/+ mice may be developmentally abnormal in comparison with WT. Detailed frequency analysis revealed that most of the USVs at P7 and P14 emitted by *patDp*/+ pups were mainly in the 50-70 kHz frequency range with some over 70 kHz, the latter of which was not seen in WT pups (Figure S9). No difference in USVs was observed between *matDp*/+ and WT pups (Figure S8C), suggesting that communicative development between dam and neonatal mice in *patDp*/+ is different from that in WT or *matDp*/+ pups. This larger number of USVs in *patDp*/+ pups may reflect higher anxiety and fear in response to stress (Crawley, 2007).

We therefore examined vocalizations in adult animals where the effects of anxiety and novel environments may be more controlled. Since adult mice emitted both audible and ultrasonic vocalizations, we measured vocalizations consisting of both frequencies. In a resident-intruder paradigm, the total number of vocalizations ranging from both audible and ultrasonic bands emitted by pairs of *patDp/+* mice were significantly decreased compared with those of a WT pair (Figure S10). The vocalizations ranging in the ultrasonic bands in pairs of *patDp/+* mice also tended to be lower than those in pairs of WT mice. The behavior between resident and intruder mice in each genotype was indistinguishable between the genotypes. These results suggest that vocal communication between pairs of *patDp/+* mice is decreased compared with a WT pair.

The fear-related behaviors of *patDp/+* mice were observed by conducting another test, the cued and contextual conditioning task by using a 60-dB white noise tone and a mild foot shock (Figures S11A-C). No significant difference in the freezing rate between *patDp/+* and WT mice was seen during conditioning training (Figure S11A) or in the same contextual environment after 24 h (Figure S11B). However,

patDp/+ mice showed higher freezing scores in the altered contextual environment than the WT controls, especially during the first 3 minutes in the absence of the cue (Figure S11C). *matDp/+* mice displayed no difference from WT mice (Figures S12A-C). These results suggest that the *patDp/+* mice show a generalized fear. Additionally, we conducted the elevated plus maze test to examine anxiety (Figures S11D-G). As compared with WT, the *patDp/+* mice showed no significant difference in distance traveled (Figure S11D); whereas the number of entries into the arms and time in the open arms were significantly decreased in the *patDp/+* mice (Figures S11E and S11F), but not in the *matDp/+* mice (Figures S12D-G). These results suggest that the *patDp/+* mice show increased anxiety, a feature common in autistic individuals (Crawley, 2004).

5-HT2c receptor signaling is altered in *patDp*/+ neurons

Our behavioral tests demonstrated that *patDp*/+ mice show abnormal behaviors. The primary benefit of the model mouse system is that it allows us to study abnormality at the molecular level. To demonstrate this possibility, we examined one molecular candidate, i.e., a small nucleolar RNA (snoRNA). It has been reported that a

brain-specific snoRNA, HBII52, the human ortholog of MBII52, plays a role in posttranscriptional modification of the serotonin 2c receptor (5-HT2cR), a G-protein-coupled receptor (GPCR) (Kishore and Stamm, 2006), which may cause amino acid substitutions in the second intracellular domain of this receptor. The 5-HT2cR is the only GPCR that has been shown to undergo physiologically important editing of its pre-mRNA by adenosine deamination (A-to-I editing), resulting in amino acid substitutions (Seeburg, 2002). We examined MBII52 RNA expression in the brain by RNA blot hybridization (Figure 6A). Since the locus including MBII52 is maternally imprinted, the expression of MBII52 in the *patDp*/+ mouse brains was approximately twice as much as that in the WT or *matDp*/+ brains. We next analyzed the editing ratio of 5-HT2cR RNA at 5 potential sites that are located in the second intracellular domain. RNA editing ratios in *patDp*/+ at the A and B sites were significantly higher than those in WT and *patDp*/+ editing ratios at the D site was higher than *matDp*/+, whereas no significant difference was found for the editing frequency at the E and C sites among the 3 types of mice (Figure S13).

Because 5-HT2cR induces an increase in the intracellular calcium level

($[Ca^{2+}]_i$) via G-proteins coupled to phospholipase C, we asked whether altered amounts of MBII52 would affect the $[Ca^{2+}]_i$ response via altered coupling efficiency between 5-HT2cR and G-proteins. To analyse the serotonergic signals in neurons derived from mouse brains, we examined the effects of 5-HT2cR on $[Ca^{2+}]_i$ in primary cultured neurons by using microspectrofluorimetric techniques and the fluorescent indicator Fura-2 (Figure 6B). A specific agonist for 5-HT2cR, WAY 161503, induced an increase in $[Ca^{2+}]_i$. The response to 100 nM WAY 161503 in *patDp*/+ neurons was significantly higher than that in WT (Figures 6C, D). These results demonstrate that substantial alterations in the amount of MBII52 RNA of the *patDp*/+ mice resulted in a significantly increased $[Ca^{2+}]_i$ response to 5-HT2cR signaling, suggesting that this alteration in serotonergic signaling may contribute to the abnormal behavior seen in the *patDp*/+ mice.

Discussion

Ideal animal models of human neuropsychiatric disorders should not only phenocopy relevant human symptoms but the phenotypes should be based on similar underlying

mechanisms acting both physiologically and genetically (Crawley, 2004). Several kinds of animal models for autism have been reported (Moy et al., 2006; Murcia et al., 2005; Persico and Bourgeron, 2006). Knockouts or knockin of single candidate genes, such as genes in the oxytocin-vasopressin system, dishevelled-1 (*Dv1*), engrailed2 (*En2*), *Pten* and neuroligins have been reported as possible autistic model mice (DiCicco-Bloom et al., 2006; Jamain et al., 2008; Kwon et al., 2006; Lijam et al., 1997; Moretti et al., 2005; Tabuchi et al., 2007; Winslow and Insel, 2002; Young, 2007). Ours mirrors a chromosomal abnormality found in human autistic patients. In this regard, the chromosome-engineered mouse described here is a model mouse for autism that parallels both phenotypic and genotypic aspects of the human disease.

In the rotarod test *patDp*/+ mice exhibited a significantly greater improvement of rotarod performance compared with WT mice (Figure S14). This result may simply mean that *patDp*/+ mice possess higher motor coordination/learning ability compared with WT mice, but taken together with the results of the reversal learning, it can be interpreted that *patDp*/+ show better stereotypic behavior. This motor stereotypy or better performance in repetitive tests of motor coordination has also been reported in

other models (Caston et al., 1998; Kwon et al., 2006). In addition to the major symptoms, there are several associated manifestations of emotional behavior in autism, such as anxiety, fear, and depression. Indeed *patDp/+* mice displayed these signs in the cued and contextual conditioning fear test, the elevated plus maze test, and the Porsolt forced swim test (Figures S11 and S15). Mao *et al.* reported that a patient with paternal duplicated 15q11-13 displayed depression and anxiety in addition to significant behavioral problems and obesity (Mao et al., 2000). Furthermore, in the eight-arm radial maze test, we noticed strange behavior in *patDp/+* mice. Even after training with dietary restriction, several mice did not seem to be eager to eat food. In addition, the latency of *patDp/+* mice to approach food was significantly longer than that of WT mice in the T-maze test. These findings might reflect the increase in latency to feed observed in the novelty-suppressed feeding (NSF) test (Santarelli et al., 2003). These behavioral phenotypes may imply that *patDp/+* mice have greater fear and tend to freeze in novel environments or have a lack of desire.

In this study, mice with a paternal duplication showed abnormal phenotypes compared with WT mice. Reports on human autism associated with a paternal

duplication have been accumulating (Bolton et al., 2004; Mao et al., 2000; Mohandas et al., 1999; Roberts et al., 2002; Veltman et al., 2005), although it has also been reported that maternal duplication of 15q11-13 causes autism in humans (Cook et al., 1997). Provided that autistic patients with the chromosome 15q11-13 duplications are the small affected cases compared with overall autistic patients, one should re-evaluate more clinical cases with the use of currently available high-resolution genome analysis techniques such as array CGH as well as multiple oligonucleotide array platforms (Lee and Lupski, 2006). Some epigenetic controls may be different between human and mouse. Although the methylation status revealed by analyzing one probe around the IC region in this study seems to be conserved also in the mouse, methylation in other regions remains unknown. Epigenetic, developmental and environmental influences may affect marked variability in phenotypic expression (Veltman et al., 2005).

The link between social behaviors in rodents and social behavior in human is difficult to establish. Our model would provide a powerful tool to explore its mechanism. It has been reported that serotonin may be involved in the pathophysiology of autism, because serotonin plays a role as a growth factor in the immature brain

(Bonnin et al., 2007; Riccio et al., 2008). Increased serotonergic activity during development could damage the neurocircuitry involved in emotional responses to social stress and may have relevance to the symptoms of autism (Whitaker-Azmitia, 2005). The 5-HT2cR studied here, mapped to the X-chromosome, may be a candidate molecule for human genetic studies of autism and its ligand may be a potential lead for therapeutic targets. Another intriguing hypothesis is imbalance between excitatory and inhibitory neural signals at the developmental stages (Dykens et al., 2004; Levitt et al., 2004; Polleux and Lauder, 2004; Rubenstein and Merzenich, 2003). In this respect, a cluster of the $GABA_A$ receptor subunits in the duplicated region and its relevance to development is of particular interest for further study. It remains possible that other genes in this duplicated region and their downstream effects may cause abnormal behavior. Systematic approaches such as using a series of BACs tiled across the region to make transgenic mice will help to resolve these questions. Our model mouse will be valuable not only for therapeutic studies but also provides a starting point for more detailed genetic analysis directed towards understanding the etiology of developmental brain disorders.

Experimental Procedures

A chromosome-engineered mouse model. The detailed procedure of the Cre/*loxP* chromosomal engineering system was described previously (Bradley and van der Weyden, 2005; Zheng et al., 1999). Genomic DNA was derived from male 129S5 mice. The 5'*hprt* (hypoxanthine phosphoribosyl transferase) library vector carries the neomycin resistance gene for gene targeting, a *loxP* site, 5'*hprt* minigene for chromosome engineering and a Tyrosinase minigene for coat color tagging. The 3'*hprt* library backbone contains the puromycin resistance gene, a *loxP* site, 3'*hprt* and an Agouti transgene under the control of the K14 promotor. Each rearrangement requires the successive targeting of two end-points with complementary halves of the *Hprt* minigene and different positive selection marker. By recombination the *Hprt* minigene is reconstituted so that cell with rearranged chromosomes can be selected by using HAT media. The 5'*hprt* and 3'*hprt* library were screened by using a 440-bp fragment between mouse *Mkrn3* and *Frat3* genes and a 930-bp fragment between *Herc2* and *Shyc* genes, respectively. Two targeting vectors were sequentially transfected into AB2.2 *hprt*-deficient ES cells by electroporation, confirming the structure of the recombinant chromosome at each step by Southern blotting after drug selection with G418 or

puromycin. The double targeted ES cells were used to induce the rearrangement. The Cre expression vector pOG231 was electroporated into these cells and the recombination products were selected using HAT medium. The clones carrying the duplication were injected into 3.5 day blastocysts from C57BL/6-*Tyr*^{cBrd}/^{cBrd} mice. Chimaeras that are generated from blastocyst injection are mated with C57BL/6-*Tyr*^{cBrd}/^{cBrd} wild-type mice to establish germline transmission of the modified genome. The experimental procedures and housing conditions for animals were approved by OBI Animal Research Committee.

CGH by BAC microarray. The mouse whole-genome BAC array used in this study contained 2,803 unique BAC clones from mouse genomic libraries spaced at 1-Mb intervals (Chung et al., 2004). Detailed conditions were included in supplemental Experimental Procedures.

Quantitative real-time reverse transcription (RT)-PCR. The quantitative assays for mRNA expression were described previously (Yamamoto et al., 2005). TaqMan® Low Density Array (Applied Biosystems), which contained mouse *Tubgcp5*, *Herc2*, *P*, *Gabrγ3*, *Gabrα5*, *Gabrβ3*, *Atp10a*, *Ube3a*, *Magel2*, *Mkrn3*, *Chrna7* and 18S rRNA

(internal control), was examined by using an ABI PRISM 7900HT Sequence Detection System (Applied Biosystems). Each quantification of relative RNA levels by the SYBR Green real-time PCR technology was done as described previously (Akashi and Takumi, 2005). The PCR primers and detailed procedures were included in supplemental Experimental Procedures.

Three-chambered social interaction. Social testing apparatus consisted of a rectangular, three-chambered box and a lid with an infrared video camera (Nadler et al., 2004) (Ohara & Co., Tokyo). Each chamber was 20 × 40 × 22 cm and the dividing walls were made from clear Plexiglas, with small square openings (5 × 3 cm) allowing access into each chamber. An unfamiliar C57BL/6J male (stranger), that had no prior contact with subject mice, was placed in one of the side chambers. The location of stranger in the left vs. right side chamber was systematically alternated between trials. The stranger mouse was enclosed in a small, round wire cage, which allowed olfactory, visual, auditory and tactile contacts but did not allow sexual and deep contacts. The subject mouse was first placed in the middle chamber and allowed to explore the entire social test box for a 10-min session. Measures were taken of the amount of time spent in

quadrant around wire cage by a camera, which is attached at the top of box. More detailed conditions were included in supplemental Experimental Procedures.

Morris water task. The visible platform, hidden platform, probe test, and reversal probe test components of the Morris water task were conducted in a circular pool, 1.0 m in diamater (Ohara & Co.). Detailed conditions were included in supplemental Experimental Procedures.

Barnes maze task. The Barnes maze task was conducted on "dry land," a white circular surface, 1.0 m in diameter, with 12 holes equally spaced around the perimeter (Miyakawa et al., 2001) (Ohara & Co.). Detailed conditions were included in supplemental Experimental Procedures.

Ultrasonic vocalization. After habituation, each pup was removed from its mother and placed in a stainless-steel cylinder (size 7.5 cm diameter x 7 cm height) on the COOL PLATE® (NCP-2215, Nisshin Rika Co., Ltd.) which maintained temperature of the cylinder at 24 ºC in a sound proof room (AT-81, RION Co., Ltd.). The number of vocalization was measured for 5 min. More detailed conditions were included in supplemental Experimental Procedures.

Calcium measurement in neuronal cell culture. The procedure for primary culture of neurons was described previously (Yoshimura et al., 2006). The neurons were prepared from embryonic mice brain at E16 and plated onto poly-L-lysine-coated glass bottom dishes. All measurements were performed with day 7-9 from preparation. To measure the intracellular calcium, primary cultured neurons were loaded with 5 μM Fura-2 acetoxymethyl ester (Dojindo) at room temperature for 30 min. Cells on a coverglass placed in a recording chamber were perfused with HEPES solution (135 mM NaCl, 5 mM KCl, 2 mM $CaCl_2$, 2 mM $MgCl_2$, 10 mM HEPES, and 10 mM glucose, adjusted at pH 7.4 with NaOH) by gravity. This chamber was mounted on the stage of an inverted fluorescence microscope (Axiovert 135, Zeiss). Various concentrations (0.1 nM, 1 nM, 10 nM, 100 nM and 1000 nM) of WAY 161503 (Rosenzweig-Lipson et al., 2006) (Tocris) were perfused for 3 min with a 10-min interval. With a digital image analysis system (MetaFluor, Molecular Devices), the fluorescence ratio (340 nm/380 nm) for each neuron was analyzed. For data analysis, the neurons displaying above 0.02 on the intensity (Δ 340 nm/380 nm) at 1 μM WAY 161503 were selected.

Statistical analysis. Statistical analysis was conducted using StatView (SAS institute).

Data were analyzed by two-way ANOVA, or two-way repeated measures ANOVA, or one-way ANOVA followed by Bonferroni-Dunn test unless noted otherwise. Values in tables and graphs were expressed as mean ± SEM.

Other methods. All the detailed procedures were included in supplemental Experimental Procedures.

Acknowledgements

TT acknowledges M. Young for discussions that led to start this project and K. Tanaka, O. Hayaishi, H. Hanafusa, and S. Nakanishi for general support. The authors thank K. Sakimura and M. Abe for their help in the initial stage of this study; N. Nakai, A. Yamamoto, T. Sudo, F. Law, A. Beasley, E. Grau, T. Hamilton, L. Davis, H. Kitson, H. Ogino, and R. Takayama for technical assistance; W. Wang, D. Adams, N. Conte, T. Kishino, T. Manabe, and P. Levitt for valuable comments and all members of the Takumi laboratory. We also thank K. Nakao and members of Animal Resource Unit, RIKEN CDB for breeding of mice. JN and ST were supported by JSPS fellowship. This work was supported in part by a grant from the Grants-in-Aid for Scientific Research on Priority Areas-Research on Pathomechanisms of Brain Disorders from the MEXT, Neuroinformatics Japan Center (NIJC), Institute for Bioinformatics Research and Development (BIRD), CREST of Japan Science and Technology Agency, and by research grants from the Mitsubishi Foundation, the Mother and Child Health Foundation, the Mitsubishi Pharma Research Foundation, the Takeda Science Foundation, the Astellas Foundation for Research on Metabolic Disorders, Sony

Corporation, Nippon Boehringer Ingelheim Co., Ltd, and the Wellcome Trust.

References

Abrahams, B.S., and Geschwind, D.H. (2008). Advances in autism genetics: on the threshold of a new neurobiology. Nat Rev Genet *9*, 341-355.

Akashi, M., and Takumi, T. (2005). The orphan nuclear receptor RORalpha regulates circadian transcription of the mammalian core-clock Bmal1. Nat Struct Mol Biol *12*, 441-448.

Beaudet, A.L. (2007). Autism: highly heritable but not inherited. Nat Med *13*, 534-536.

Belmonte, M.K., Cook, E.H., Jr., Anderson, G.M., Rubenstein, J.L., Greenough, W.T., Beckel-Mitchener, A., Courchesne, E., Boulanger, L.M., Powell, S.B., Levitt, P.R.*, et al.* (2004). Autism as a disorder of neural information processing: directions for research and targets for therapy. Mol Psychiatry *9*, 646-663.

Bolton, P.F., Veltman, M.W., Weisblatt, E., Holmes, J.R., Thomas, N.S., Youings, S.A., Thompson, R.J., Roberts, S.E., Dennis, N.R., Browne, C.E.*, et al.* (2004). Chromosome 15q11-13 abnormalities and other medical conditions in individuals with autism spectrum disorders. Psychiatr Genet *14*, 131-137.

Bonnin, A., Torii, M., Wang, L., Rakic, P., and Levitt, P. (2007). Serotonin modulates

the response of embryonic thalamocortical axons to netrin-1. Nat Neurosci *10*, 588-597.

Bradley, A., and van der Weyden, L. (2005). Mouse: Chromosome Engineering for Modeling Human Disease. Annu Rev Genomics Hum Genet *7*, 247-276.

Caston, J., Yon, E., Mellier, D., Godfrey, H.P., Delhaye-bouchaud, N., and Mariani, J. (1998). An animal model of autism: behavioural studies in the GS guinea-pig. Eur J Neurosci *10*, 2677-2684.

Chung, Y.J., Jonkers, J., Kitson, H., Fiegler, H., Humphray, S., Scott, C., Hunt, S., Yu, Y., Nishijima, I., Velds, A.*, et al.* (2004). A whole-genome mouse BAC microarray with 1-Mb resolution for analysis of DNA copy number changes by array comparative genomic hybridization. Genome Res *14*, 188-196.

Cook, E.H., Jr., Lindgren, V., Leventhal, B.L., Courchesne, R., Lincoln, A., Shulman, C., Lord, C., and Courchesne, E. (1997). Autism or atypical autism in maternally but not paternally derived proximal 15q duplication. Am J Hum Genet *60*, 928-934.

Cook, E.H., Jr., and Scherer, S.W. (2008). Copy-number variations associated with neuropsychiatric conditions. Nature *455*, 919-923.

Crawley, J.N. (2004). Designing mouse behavioral tasks relevant to autistic-like

behaviors. Ment Retard Dev Disabil Res Rev *10*, 248-258.

Crawley, J.N. (2007). What's wrong with my mouse?, 2nd edn (New York, John Wiley & Sons, Inc.).

DiCicco-Bloom, E., Lord, C., Zwaigenbaum, L., Courchesne, E., Dager, S.R., Schmitz, C., Schultz, R.T., Crawley, J., and Young, L.J. (2006). The developmental neurobiology of autism spectrum disorder. J Neurosci *26*, 6897-6906.

Dykens, E.M., Sutcliffe, J.S., and Levitt, P. (2004). Autism and 15q11-q13 disorders: behavioral, genetic, and pathophysiological issues. Ment Retard Dev Disabil Res Rev *10*, 284-291.

Folstein, S.E., and Rosen-Sheidley, B. (2001). Genetics of autism: complex aetiology for a heterogeneous disorder. Nat Rev Genet *2*, 943-955.

Geschwind, D.H. (2008). Autism: many genes, common pathways? Cell *135*, 391-395.

Geschwind, D.H., and Levitt, P. (2007). Autism spectrum disorders: developmental disconnection syndromes. Curr Opin Neurobiol *17*, 103-111.

Geurts, H.M., Corbett, B., and Solomon, M. (2009). The paradox of cognitive flexibility in autism. Trends Cogn Sci *13*, 74-82.

Jamain, S., Radyushkin, K., Hammerschmidt, K., Granon, S., Boretius, S., Varoqueaux, F., Ramanantsoa, N., Gallego, J., Ronnenberg, A., Winter, D., *et al.* (2008). Reduced social interaction and ultrasonic communication in a mouse model of monogenic heritable autism. Proc Natl Acad Sci U S A *105*, 1710-1715.

Kishore, S., and Stamm, S. (2006). The snoRNA HBII-52 regulates alternative splicing of the serotonin receptor 2C. Science *311*, 230-232.

Kwon, C.H., Luikart, B.W., Powell, C.M., Zhou, J., Matheny, S.A., Zhang, W., Li, Y., Baker, S.J., and Parada, L.F. (2006). Pten regulates neuronal arborization and social interaction in mice. Neuron *50*, 377-388.

Lee, J.A., and Lupski, J.R. (2006). Genomic rearrangements and gene copy-number alterations as a cause of nervous system disorders. Neuron *52*, 103-121.

Levitt, P., Eagleson, K.L., and Powell, E.M. (2004). Regulation of neocortical interneuron development and the implications for neurodevelopmental disorders. Trends Neurosci *27*, 400-406.

Lijam, N., Paylor, R., McDonald, M.P., Crawley, J.N., Deng, C.X., Herrup, K., Stevens, K.E., Maccaferri, G., McBain, C.J., Sussman, D.J., *et al.* (1997). Social interaction and

sensorimotor gating abnormalities in mice lacking Dvl1. Cell *90*, 895-905.

Lord, C., Cook, E.H., Leventhal, B.L., and Amaral, D.G. (2000). Autism spectrum disorders. Neuron *28*, 355-363.

Maestrini, E., Paul, A., Monaco, A.P., and Bailey, A. (2000). Identifying autism susceptibility genes. Neuron *28*, 19-24.

Mao, R., Jalal, S.M., Snow, K., Michels, V.V., Szabo, S.M., and Babovic-Vuksanovic, D. (2000). Characteristics of two cases with dup(15)(q11.2-q12): one of maternal and one of paternal origin. Genet Med *2*, 131-135.

Miyakawa, T., Yared, E., Pak, J.H., Huang, F.L., Huang, K.P., and Crawley, J.N. (2001). Neurogranin null mutant mice display performance deficits on spatial learning tasks with anxiety related components. Hippocampus *11*, 763-775.

Mohandas, T.K., Park, J.P., Spellman, R.A., Filiano, J.J., Mamourian, A.C., Hawk, A.B., Belloni, D.R., Noll, W.W., and Moeschler, J.B. (1999). Paternally derived de novo interstitial duplication of proximal 15q in a patient with developmental delay. Am J Med Genet *82*, 294-300.

Moretti, P., Bouwknecht, J.A., Teague, R., Paylor, R., and Zoghbi, H.Y. (2005).

Abnormalities of social interactions and home-cage behavior in a mouse model of Rett syndrome. Hum Mol Genet *14*, 205-220.

Moy, S.S., Nadler, J.J., Magnuson, T.R., and Crawley, J.N. (2006). Mouse models of autism spectrum disorders: the challenge for behavioral genetics. Am J Med Genet C Semin Med Genet *142*, 40-51.

Murcia, C.L., Gulden, F., and Herrup, K. (2005). A question of balance: a proposal for new mouse models of autism. Int J Dev Neurosci *23*, 265-275.

Nadler, J.J., Moy, S.S., Dold, G., Trang, D., Simmons, N., Perez, A., Young, N.B., Barbaro, R.P., Piven, J., Magnuson, T.R.*, et al.* (2004). Automated apparatus for quantitation of social approach behaviors in mice. Genes Brain Behav *3*, 303-314.

Nicholls, R.D., and Knepper, J.L. (2001). Genome organization, function, and imprinting in Prader-Willi and Angelman syndromes. Annu Rev Genomics Hum Genet *2*, 153-175.

Noirot, E. (1966). Ultra-sounds in young rodents. I. Changes with age in albino mice. Anim Behav *14*, 459-462.

Persico, A.M., and Bourgeron, T. (2006). Searching for ways out of the autism maze:

genetic, epigenetic and environmental clues. Trends Neurosci *29*, 349-358.

Polleux, F., and Lauder, J.M. (2004). Toward a developmental neurobiology of autism. Ment Retard Dev Disabil Res Rev *10*, 303-317.

Ramocki, M.B., and Zoghbi, H.Y. (2008). Failure of neuronal homeostasis results in common neuropsychiatric phenotypes. Nature *455*, 912-918.

Riccio, O., Potter, G., Walzer, C., Vallet, P., Szabo, G., Vutskits, L., Kiss, J.Z., and Dayer, A.G. (2008). Excess of serotonin affects embryonic interneuron migration through activation of the serotonin receptor 6. Mol Psychiatry.

Roberts, S.E., Dennis, N.R., Browne, C.E., Willatt, L., Woods, G., Cross, I., Jacobs, P.A., and Thomas, S. (2002). Characterisation of interstitial duplications and triplications of chromosome 15q11-q13. Hum Genet *110*, 227-234.

Rosenzweig-Lipson, S., Zhang, J., Mazandarani, H., Harrison, B.L., Sabb, A., Sabalski, J., Stack, G., Welmaker, G., Barrett, J.E., and Dunlop, J. (2006). Antiobesity-like effects of the 5-HT2C receptor agonist WAY-161503. Brain Res *1073-1074*, 240-251.

Rubenstein, J.L., and Merzenich, M.M. (2003). Model of autism: increased ratio of excitation/inhibition in key neural systems. Genes Brain Behav *2*, 255-267.

Santarelli, L., Saxe, M., Gross, C., Surget, A., Battaglia, F., Dulawa, S., Weisstaub, N., Lee, J., Duman, R., Arancio, O., *et al.* (2003). Requirement of hippocampal neurogenesis for the behavioral effects of antidepressants. Science *301*, 805-809.

Sebat, J., Lakshmi, B., Malhotra, D., Troge, J., Lese-Martin, C., Walsh, T., Yamrom, B., Yoon, S., Krasnitz, A., Kendall, J., *et al.* (2007). Strong association of de novo copy number mutations with autism. Science *316*, 445-449.

Seeburg, P.H. (2002). A-to-I editing: new and old sites, functions and speculations. Neuron *35*, 17-20.

Tabuchi, K., Blundell, J., Etherton, M.R., Hammer, R.E., Liu, X., Powell, C.M., and Sudhof, T.C. (2007). A neuroligin-3 mutation implicated in autism increases inhibitory synaptic transmission in mice. Science *318*, 71-76.

Takao, K., Yamasaki, N., and Miyakawa, T. (2007). Impact of brain-behavior phenotypying of genetically-engineered mice on research of neuropsychiatric disorders. Neurosci Res *58*, 124-132.

Veenstra-VanderWeele, J., Christian, S.L., and Cook, E.H., Jr. (2004). Autism as a paradigmatic complex genetic disorder. Annu Rev Genomics Hum Genet *5*, 379-405.

Veenstra-VanderWeele, J., and Cook, E.H., Jr. (2004). Molecular genetics of autism spectrum disorder. Mol Psychiatry *9*, 819-832.

Veltman, M.W., Thompson, R.J., Craig, E.E., Dennis, N.R., Roberts, S.E., Moore, V., Brown, J.A., and Bolton, P.F. (2005). A paternally inherited duplication in the Prader-Willi/Angelman syndrome critical region: a case and family study. J Autism Dev Disord *35*, 117-127.

Volkmar, F.R., and Pauls, D. (2003). Autism. Lancet *362*, 1133-1141.

Vorstman, J.A., Staal, W.G., van Daalen, E., van Engeland, H., Hochstenbach, P.F., and Franke, L. (2006). Identification of novel autism candidate regions through analysis of reported cytogenetic abnormalities associated with autism. Mol Psychiatry *11*, 1, 18-28.

Whitaker-Azmitia, P.M. (2005). Behavioral and cellular consequences of increasing serotonergic activity during brain development: a role in autism? Int J Dev Neurosci *23*, 75-83.

Winslow, J.T., and Insel, T.R. (2002). The social deficits of the oxytocin knockout mouse. Neuropeptides *36*, 221-229.

Yamamoto, T., Nakahata, Y., Tanaka, M., Yoshida, M., Soma, H., Shinohara, K., Yasuda,

A., Mamine, T., and Takumi, T. (2005). Acute physical stress elevates mouse period1 mRNA expression in mouse peripheral tissues via a glucocorticoid-responsive element. J Biol Chem *280*, 42036-42043.

Yamasaki, N., Maekawa, M., Kobayashi, K., Kajii, Y., Maeda, J., Soma, M., Takao, K., Tanda, K., Ohira, K., Toyama, K.*, et al.* (2008). Alpha-CaMKII deficiency causes immature dentate gyrus, a novel candidate endophenotype of psychiatric disorders. Molecular Brain.

Yoshimura, A., Fujii, R., Watanabe, Y., Okabe, S., Fukui, K., and Takumi, T. (2006). Myosin-Va facilitates the accumulation of mRNA/protein complex in dendritic spines. Curr Biol *16*, 2345-2351.

Young, L.J. (2007). Regulating the social brain: a new role for CD38. Neuron *54*, 353-356.

Zheng, B., Mills, A.A., and Bradley, A. (1999). A system for rapid generation of coat color-tagged knockouts and defined chromosomal rearrangements in mice. Nucleic Acids Res *27*, 2354-2360.

Legends for figures

Figure 1. Human chromosome 15q11-13 and mouse chromosome 7. Schematic representation of the genomic regions in the human and mouse genomes. Details of conserved linkage in human 15q11-13 and mouse chromosome 7 are shown. The paternally, maternally expressed, and non-imprinting genes were labeled with blue, red, and green, respectively. The 2 arrowheads (BP) represent the common breakpoints; and the 2 arrows, the targeting sites of 2 loxP sequences. Genomic segments that show linkage conservation (i.e., identical gene order) in humans and mice are connected by dark shading if the gene orders are in the same direction relative to their respective centromeres. If the gene orders in the syntenic segments are in opposite orientations, they are connected by light shading.

Figure 2. Engineering an interstitial duplication on chromosome 7. (A) Insertional double targeting and genomic coordinates NCBI build m37. S = *Sac*I, T = *Tth*111I. **(B)** Southern blot analysis of ES cell DNA samples. **(C)** Cre/*loxP* recombination generates duplication and deletion chromosomes. **(D)** Southern blot analysis of ES cell DNA

confirming the duplication. **(E)** Confirmation by FISH. The probes used are shown on the left. The red and green bars represent the probes located within and outside the duplicated region, respectively. The white arrow and arrowhead represent the *Dp* and *Df* allele, respectively. **(F)** A BAC array-CGH profile of chromosome 7 from mice with the duplication. Log2-transformed hybridization ratios of duplicated mouse DNA vs WT DNA are plotted.

Figure 3. Gene expression in mice with the duplicaiton. (A) Expected gene expression levels in wild-type (WT), paternal duplication (*patDp*/+), and maternal duplication (*matDp*/+) mice. **(B)** mRNA expression in the mouse adult brain of the listed genes analyzed by quantitative RT-PCR. The relative expression levels of *patDp*/+ (n=4) and *matDp*/+ (n=4) were compared with WT (n=7) normalized to 1.0. Blue, red, and green indicate paternally-expressed, maternally-expressed genes, and non-imprinted genes, respectively. Dotted lines show the boundaries of the chromosomal rearrangement. Error bars indicate SEM (standard error of the mean). **, $p<0.0001$, *, $p<0.05$. **(C)** *Snrpn*, *Ube3a*, and *Gabrα5* mRNA expression in the adult mouse brain (top

row) and hippocampus (other rows) detected by *in situ* hybridization. Scale bars; 2 mm (top row) and 200 μm (other rows) **(D)** Methylation analysis by Southern blotting. Me, methylated; UnMe, unmethylated.

Figure 4. *patDp*/+ mice show social abnormalities. (A to **E)** Three chamber test, (**A**) Schematic representaion of the 3-chambered apparatus. The quadrant-like spaces between the full and dotted lines were used for quantitative analysis. (**B**) A stranger mouse is restricted in one of the side chambers in a wire cage, and only an empty wire cage is placed in the opposite chamber. Comparison of time spent in the quadrant spaces between "Stranger" and "Cage" for WT (n=14) and *patDp*/+ mice (n=13). Error bars, SEM. *, $p<0.05$. (**C**) A novel object A (a dodecahedral pole) is placed in a cage in the chamber on one side and no object in the chamber on the other side. Both WT and *patDp/*+ mice spent more time around the cage with a novel object. n=11. **, $p<0.001$. (**D**) Another novel object B (a cone) is placed in a cage in the chamber on one side and an adult conspecific mouse (C57BL/6J) that has had no previous contact with the subject (test mouse) in a cage in the chamber on the other side. WT mice spent more

time around the stranger mouse. n=11. *, $p<0.05$. (**E**) A novel stranger mouse (C57BL/6J) is placed in a cage in the chamber on one side and a familiar mouse that was used in a previous test in D is placed in the chamber on the other side. n=11. These data were evaluated by the *t*-test. **(F)** Maternal separation-induced ultrasonic vocalizations at P5, 7, 14, and 21 (or 22). n=32, 40, 40, and 16, respectively for *patDp*/+; n=24, 39, 39, and 12, respectively for WT. Error bars, SEM. **, $p<0.005$.

Figure 5. *patDp/+* mice showed behavioral inflexibility in the Morris water maze and Barnes maze tests. (**A** to **F**) Morris water maze test, n=20 for both genotypes. White bar, WT; black bar, *patDp/+*. (**A**) The configuration of the four quadrants in the probe test after the original training (TA, target quadrant; OP, opposite quadrant; AR, adjacent right quadrant; AL, adjacent left quadrant). (**B**), (**C**) Probe test after the original training. Upper panels indicate averaged swimming traces of the swim pattern for WT (B) and *patDp/+* mice (C). Warmer color represents more time spent. Lower panels show the quadrant occupancy for WT (B) and *patDp/+* mice (C). Both WT and *patDp/+* mice showed significantly more time spent in the target quadrant compared

with the other quadrants [WT, $F_{(3,76)}$ = 12.86, p<0.0001; *patDp/+*, $F_{(3,76)}$ = 13.31, p<0.0001; Newman-Keuls *post hoc* comparison (trained quadrant more than all the other quadrants); p<0.01 for both genotypes]. (**D**) The configuration of the four quadrants in the reversal probe test. (**E**), (**F**) Reversal probe test. Upper panels indicate averaged swimming traces of the swim pattern for WT (E) and *patDp/+* mice (F). Lower panels show the quadrant occupancy for WT (E) and *patDp/+* (F). While WT mice spent significantly more time in the reversed target quadrant, *patDp/+* mice showed no significant difference in the time spent between the quadrants [WT, $F_{(3,76)}$ = 8.20, p<0.0001; *patDp/+*, $F_{(3,76)}$ = 2.40, p=0.0745; Neuman-Keuls *post hoc* comparison (trained quadrant more than all the other quadrants); WT, p<0.01; *patDp/+*, p>0.05]. (**G** to **L**) Barnes maze test, n=22 for both genotypes. White bar, WT; black bar, *patDp/+*. (**G**) The target position in the Barnes maze original probe test. The hole at 0 degrees is the correct hole chosen as the target. (**H**), (**I**) Both genotypes could learn the target position spatially in the original probe test [WT, $F_{(11,252)}$ = 25.47, p<0.0001; *patDp/+*, $F_{(11,252)}$ = 32.27, p<0.0001; Bonferroni *post hoc* comparison (time spent around the target position more than those of all the other holes), both genotypes, p<0.01]. (**J**) The

target position in the Barnes maze reversal probe test. The target at 0 degrees is moved to the opposite position. The original target position is labeled in red, at 180 degrees, and the new target position is labeled in blue, at 0 degrees. (**K**), (**L**) While WT mice could learn the new target position flexibly, *patDp/+* mice could not respond as flexibly as WT mice [WT, $F_{(11,252)}$ = 29,08, p<0.0001; *patDp/+*, $F_{(11,252)}$ = 16.04, p<0.0001; Bonferroni post hoc comparison (target vs 180 degrees), WT, p<0.01; patDp/+, p>0.05]. *, p<0.01; n.s., not significant (p > 0.05). Furthermore, time spent around the 180 degrees position and its neighboring 150 degrees position was increased in *patDp/+* mice compared to WT (180 degrees, p<0.1; 150 degrees, p<0.05).

Figure 6 $[Ca^{2+}]_i$ response by a 5-HT2cR agonist in neurons. (A) Northern blot analysis of MBII52. Quantitative data are shown in the right panel where MBII52 expression in WT is defined as 1. **(B** to **D)** The effect of WAY 161503 on $[Ca^{2+}]_i$ in primary cultured neurons. Representative images (responding cells are indicated by an arrowhead) and average responses under various concentrations of agonist are shown in "**B**" and "**C**", respectively. Averaged data for the concentration-dependent effect of

WAY 161503 are indicated in "**D**". Error bars, SEM. n=17 for *patDp*/+, n=15 for *matDp*/+, n=18 for WT. **, $p<0.001$.

Fig. 1

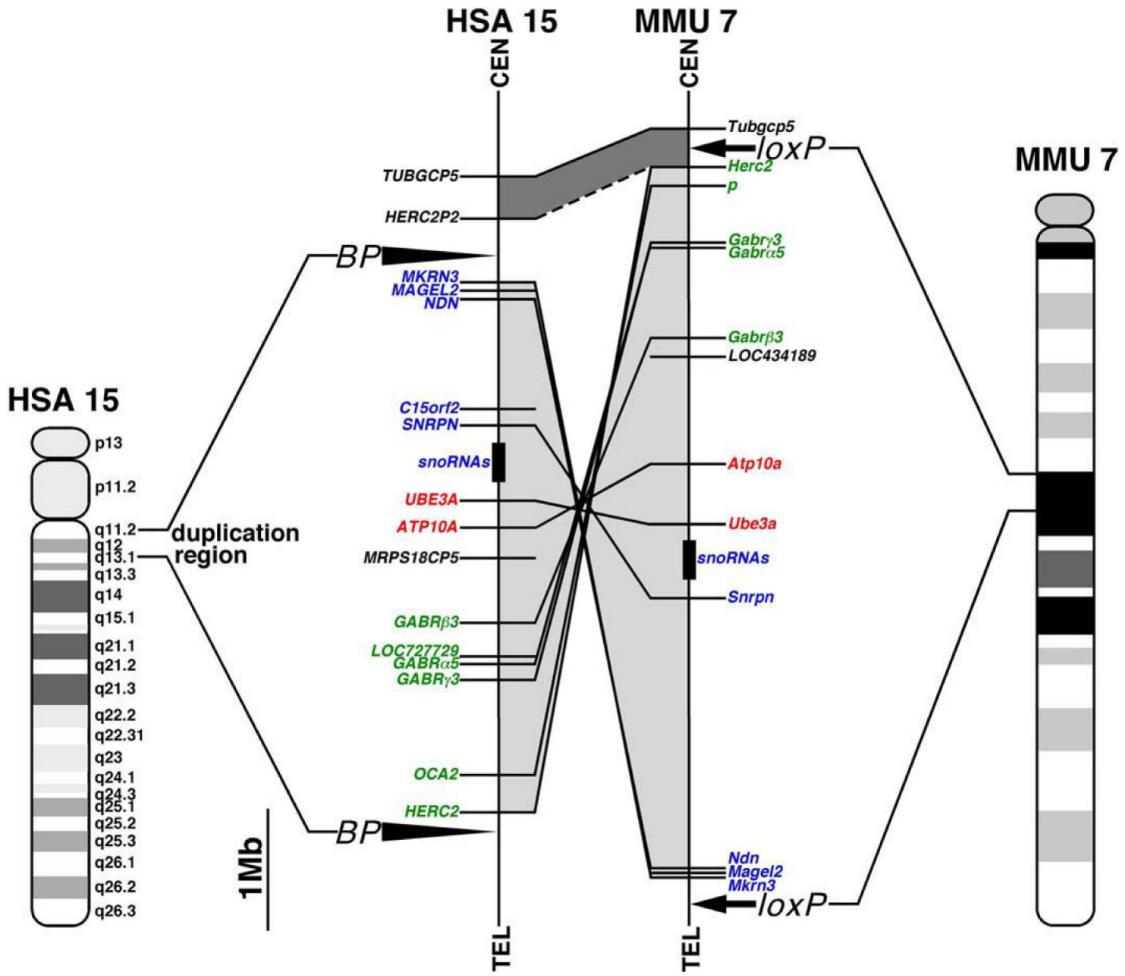
HSA 15
MMU 7
CEN
CEN
Tubgcp5
loxP
Herc2
p
TUBGCP5
HERC2P2
BP
Gabrγ3
Gabrα5
MKRN3
MAGEL2
NDN
Gabrβ3
LOC434189
C15orf2
SNRPN
snoRNAs
Atp10a
UBE3A
ATP10A
Ube3a
MRPS18CP5
snoRNAs
Snrpn
GABRβ3
LOC727729
GABRα5
GABRγ3
OCA2
HERC2
BP
1Mb
Ndn
Magel2
Mkrn3
loxP
TEL
TEL
MMU 7
HSA 15
p13
p11.2
q11.2
q12
q13.1
q13.3
q14
q15.1
q21.1
q21.2
q21.3
q22.2
q22.31
q23
q24.1
q24.3
q25.1
q25.2
q25.3
q26.1
q26.2
q26.3
duplication
region

Fig. 2

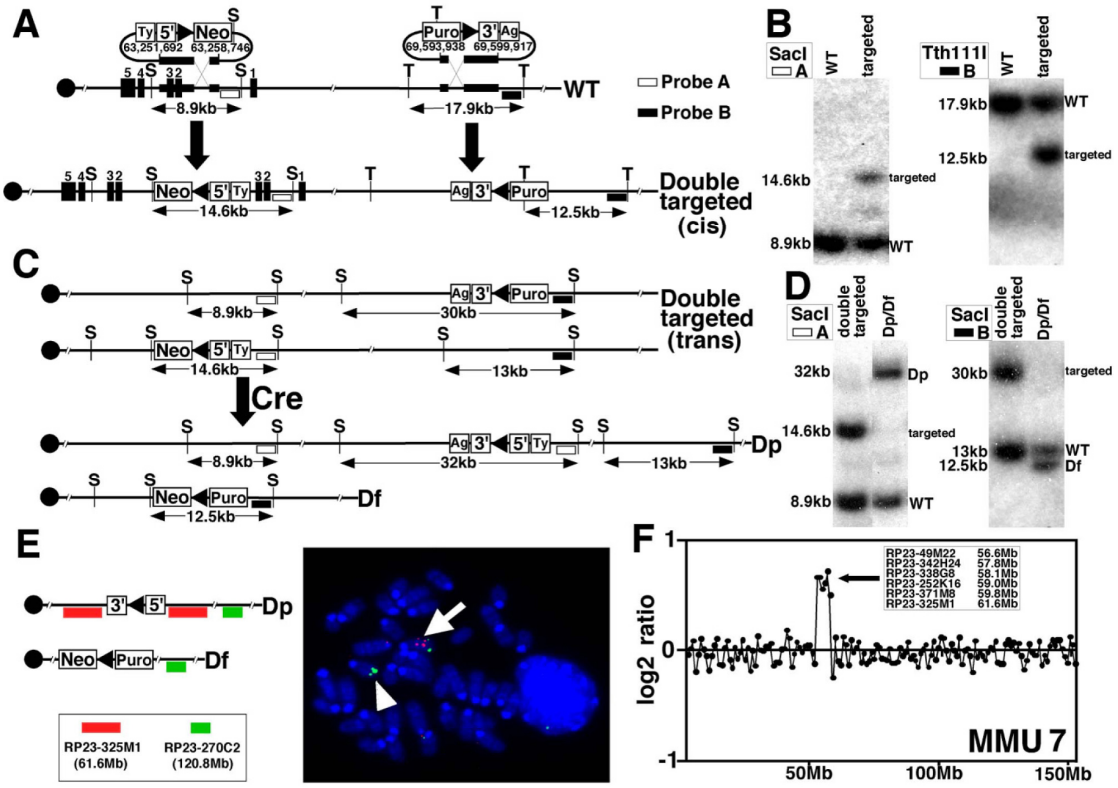
A
Ty
5'
Neo
63,251,692
63,258,746
Puro
3'
Ag
69,593,938
69,599,917
WT
8.9kb
17.9kb
Probe A
Probe B
Double targeted (cis)
14.6kb
12.5kb
B
SacI
A
WT
targeted
14.6kb
8.9kb
Tth111I
B
17.9kb
12.5kb
C
Double targeted (trans)
30kb
13kb
Cre
Dp
Df
D
double targeted
Dp/Df
32kb
30kb
E
RP23-325M1 (61.6Mb)
RP23-270C2 (120.8Mb)
F
log2 ratio
RP23-49M22 56.6Mb
RP23-342H24 57.8Mb
RP23-338G8 58.1Mb
RP23-252K16 59.0Mb
RP23-371M6 59.8Mb
RP23-325M1 61.6Mb
MMU 7
50Mb
100Mb
150Mb

Fig. 3

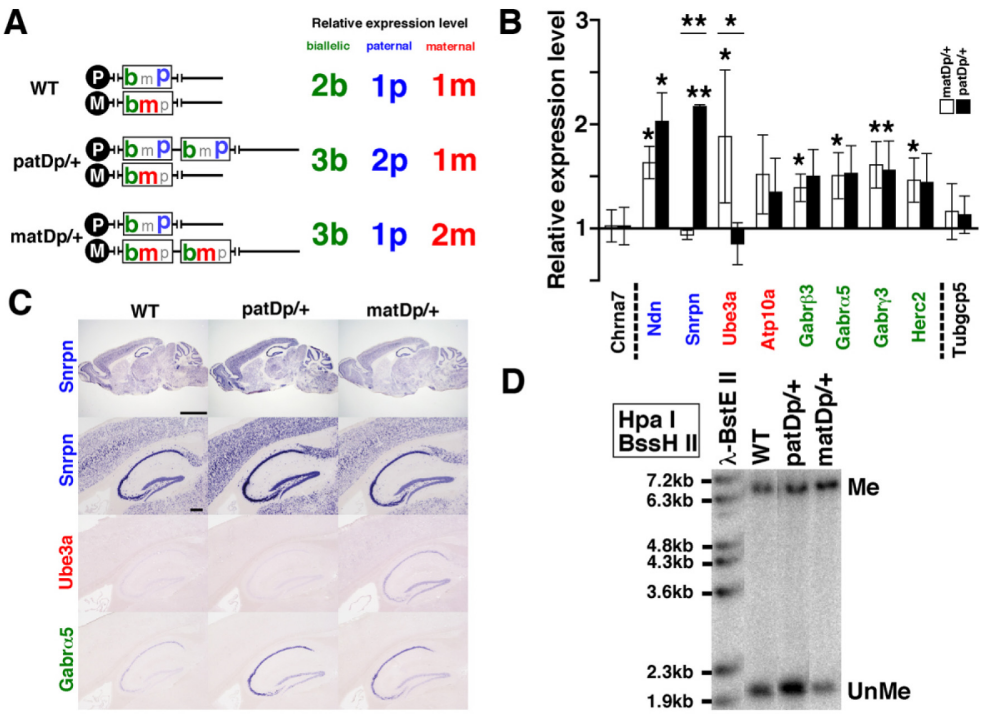
A
Relative expression level
biallelic paternal maternal
WT
2b 1p 1m
patDp/+
3b 2p 1m
matDp/+
3b 1p 2m
B
Relative expression level
matDp/+
patDp/+
Chrna7
Ndn
Snrpn
Ube3a
Atp10a
Gabrβ3
Gabrα5
Gabrγ3
Herc2
Tubgcp5
C
WT
patDp/+
matDp/+
Snrpn
Snrpn
Ube3a
Gabrα5
D
Hpa I
BssH II
λ-BstE II
WT
patDp/+
matDp/+
7.2kb
6.3kb
4.8kb
4.3kb
3.6kb
2.3kb
1.9kb
Me
UnMe

Fig. 4

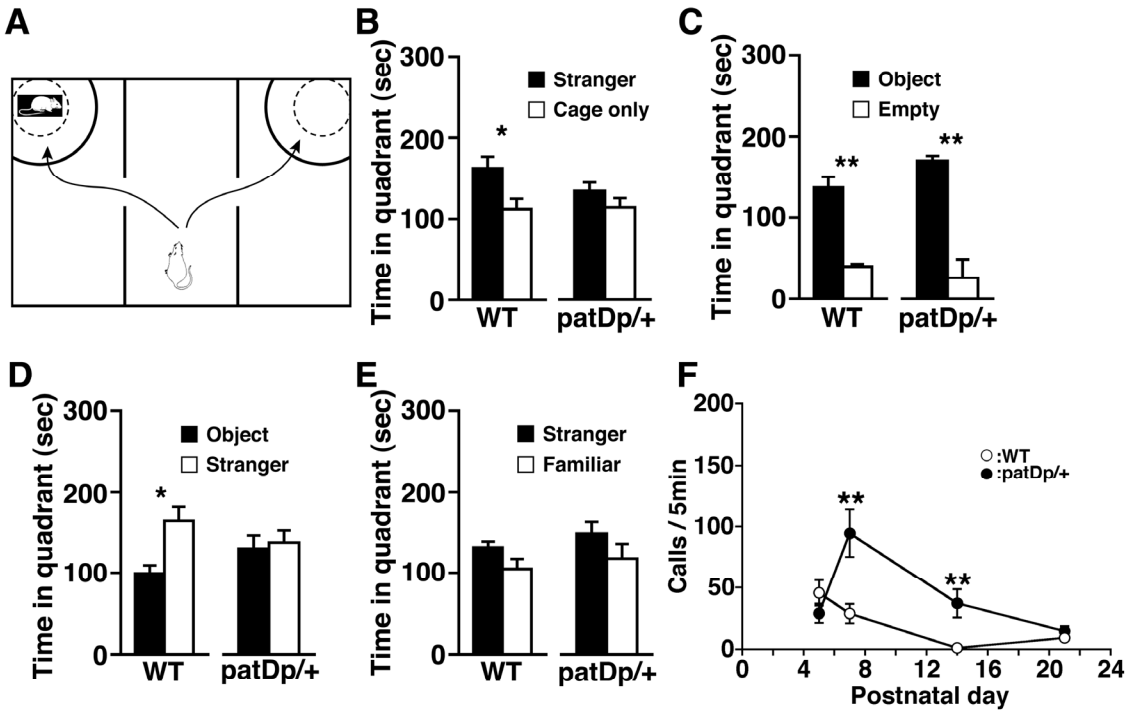
A
B
Time in quadrant (sec)
300
200
100
0
Stranger
Cage only
*
WT
patDp/+
C
Time in quadrant (sec)
Object
Empty
**
**
WT
patDp/+
D
Time in quadrant (sec)
Object
Stranger
*
WT
patDp/+
E
Time in quadrant (sec)
Stranger
Familiar
WT
patDp/+
F
Calls / 5min
200
150
100
50
0
:WT
:patDp/+
**
**
0
4
8
12
16
20
24
Postnatal day

Fig, 5

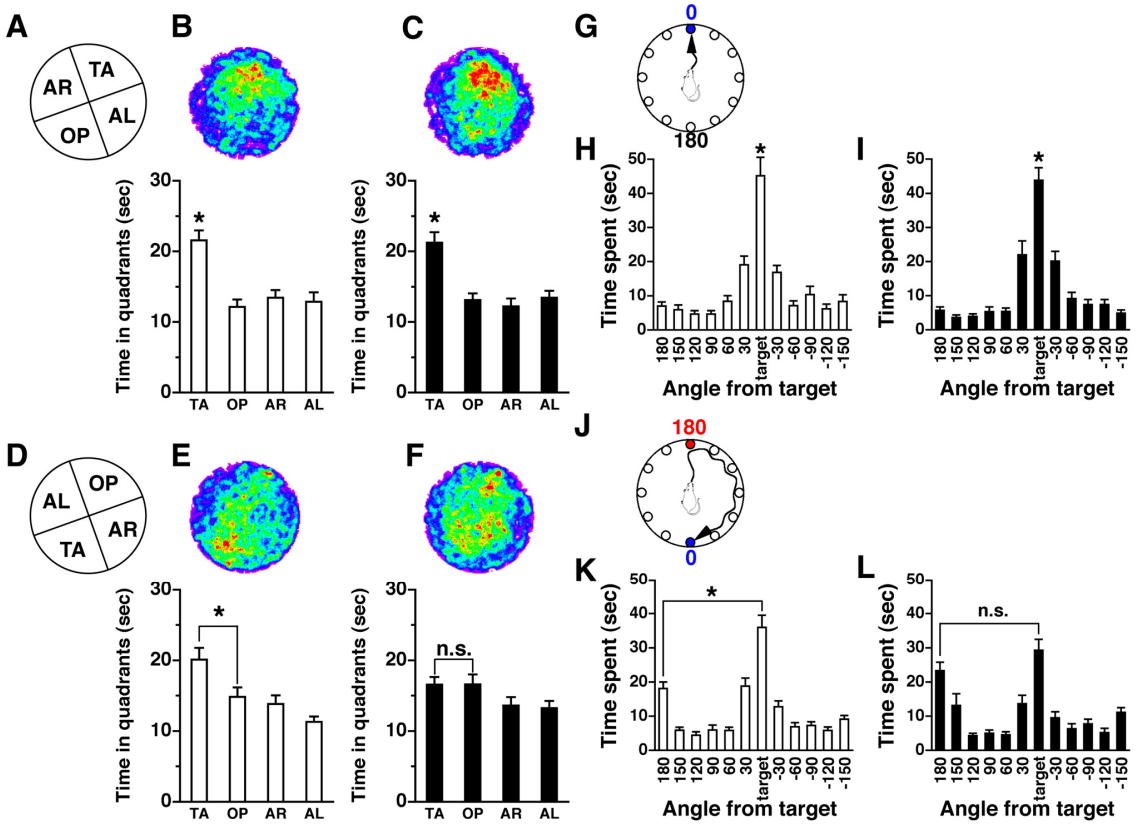
A
TA
AR
AL
OP
B
C
Time in quadrants (sec)
TA OP AR AL
G
0
180
H
I
Time spent (sec)
Angle from target
D
E
F
J
K
L
n.s.

Fig. 6

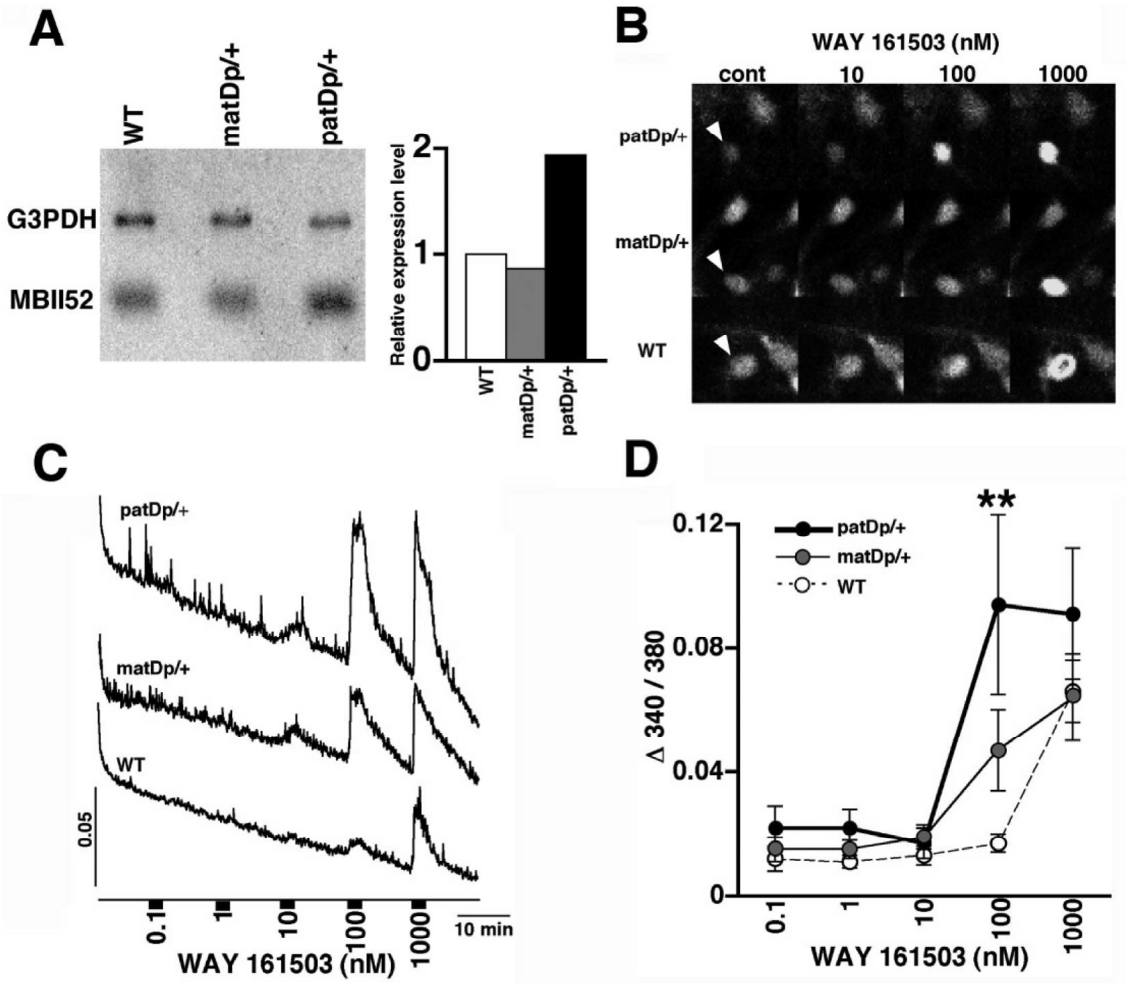
A
WT
matDp/+
patDp/+
G3PDH
MBII52
Relative expression level
2
1
0
WT
matDp/+
patDp/+
B
WAY 161503 (nM)
cont
10
100
1000
patDp/+
matDp/+
WT
C
patDp/+
matDp/+
WT
0.05
0.1
1
10
100
1000
10 min
WAY 161503 (nM)
D
**
0.12
0.08
0.04
0
Δ 340 / 380
patDp/+
matDp/+
WT
0.1
1
10
100
1000
WAY 161503 (nM)

Supplemental Experimental Procedures

Southern blot. Genomic DNAs were isolated from mouse ES cells by the proteinase K/SDS digestion. DNA was electrophoresed on a 0.8% agarose gel and transferred to a Hybond-N+ membrane (Amersham). The membrane was hybridized with α^{32}P-dCTP labeled probes at 65 ^{o}C. The DNA probes used were a 330-bp fragment between mouse *Herc2* and *Shyc* genes (probe A) and a 700-bp fragment between *Mkrn3* and *Peg12* (probe B). The filter was washed in 0.6x SSC and 1% SDS at 65 ^{o}C.

Animals. The original experiments except the following ones were conducted by using 129SvEv background mice (Figure 2, 3, S1-4, S6-8, S11-12, S14-15). Mice backcrossed with C57BL/6J were used in 3-chamber test, Morris water maze task, Barnes maze test, all USV tests, T-maze test, olfactory immunohistochemistry, and olfactory habituation/dishabituation test (Figure 4, 5, 6, S5, S9-10, S13).

Fluorescence *in situ* hybridization (FISH). Chromosome spreads of ES cells for hybridization were prepared as described (Robertson, 1987). RP23-325M1 was labeled with biotin and detected avidin-Texas Red. RP23-270C2 was labeled with digoxigenin and detected by anti-digoxigenin-FITC.

CGH by BAC microarray. Genomic DNA was extracted and purified by standard protocol. Test DNA and control DNA were digested with *Hae*III for 2 h. Digested genomic DNA was labeled with Cy3- or Cy5-dCTP by random priming (BioPrime DNA Labeling Kit, Invitrogen). Hybridization was performed in humid chamber on an orbital shaker for 48 h at 37 ^{o}C. Slides were washed in PBS containing 0.05% Tween 20 for 10 min at room temperature, next in 50% formamide 2x SSC at 42 ^{o}C for 30 min, and last in same condition as first wash. Finally, slides were spin-dried for 3 min at 1000 rpm.

Quantitative real-time reverse transcription (RT)-PCR. For one port of the TaqMan Low Density Array, 100 ng cDNA template was mixed with 50 μl of 2x TaqMan Universal PCR Master Mix (Applied Biosystems) and filled up to 100 μl with distilled water. The reaction was first incubated at 50 ^{o}C for 2 min, then at 95 ^{o}C for 10 min, followed by 40 cycles of 95 ^{o}C for 15 sec and 60 ^{o}C for 1 min. The PCR primers for the SYBR Green real-time PCR were designed with Primer express software (Applied Biosystems), and sequences of primers were as follows: *Ndn* FW: 5'-GTA TCC CAA ATC CAC AGT GC-3', *Ndn* RV: 5'-TAA CTC TCC AGG GCC TTC TT-3', *Snrpn* FW: 5'-GCA AAA CAG CCA GAA CGT GAA-3', *Snrpn* RV: 5'-GCA CAC GAG CAA

TGC CAG TAT-3', 18S rRNA FW: CGC CGC TAG AGG TGA AAT TC, 18S rRNA RV: CGA ACC TCC GAC TTT CGT TCT, 18S rRNA TaqMan probe: CCG GCG CAA GAC GGA CCA GA. For a 25-μl PCR reaction, 50 ng cDNA template was mixed with the primers and probe to final concentrations of 300 nM and 2 nM, respectively, and 12.5 μl of 2x TaqMan PCR Master Mix (Applied Biosystems). The reaction was first incubated at 50 °C for 2 min, then at 95 °C for 10 min, followed by 40 cycles of 95 °C for 15 sec and 60 °C for 1 min.

in situ **hybridization.** The procedure was performed as following our previous report (Inoue et al., 2004). The 10-week-old C57BL/6J mice were sacrificed by cervical dislocation, and their brains were removed, immediately frozen in powdered dry ice, and stored at –70 °C. Twenty μm cryosections were cut on a cryostat at –15 °C and mounted onto APS-coated slides (Matsunami, Osaka). Slides were stored at –20 °C until use. Template DNAs for probes were synthesized by PCR using specific primers and mouse brain cDNA. Digoxigenin (DIG)-labeled RNA probes were synthesized by *in vitro* transcription using sequence for *Snrpn* (the sequence corresponding to the nucleotides 449-1187 of Gene accession number NM-013670; for *Ube3a*, nucleotides

678-1371 of NM-011668; for *Gabrα5*, nucleotides 343-1250 of NM-176942) as templates. In addition, sense probe for the templates was synthesized as negative control. Sections were fixed with 4% paraformaldehyde in phosphate buffered saline (PBS) pH 7.4, treated with proteinase K (5 μg/ml) for 3 min, fixed with 4% paraformaldehyde/0.2% glutaraldehyde in PBS for 15 min, and prehybridized at 70 ^{o}C for 1 h with hybridization buffer (50% formamide, 5x SSC, 50 μg/ml yeast tRNA, 1% SDS, and 50 μg/ml heparin). The sections were then incubated for 12 h at 70 ^{o}C in the same hybridization buffer containing the DIG-labeled probe. The sections were washed with 50% formamide, 5x SSC, 1% SDS at 70 ^{o}C for 45 min, 50% formamide, 2x SSC at 65 ^{o}C for 45 min, and Tris-buffered saline containing 0.1% Tween-20 (TBST) for 30 min. The sections were subsequently incubated in 0.5% blocking reagent (Roche Diagnostics, Basel, Switzerland) in TBST for 1 h, and in the same solution containing an alkaline phosphatase-conjugated anti-DIG antibody (Roche Diagnostics) at 1:2000 for 4 h. Sections were next washed in TBST, and then in 100 mM NaCl, 100 mM Tris-HCl, pH 9.5, 50 mM $MgCl_2$, 0.1% Tween-20 (NTMT). Sections were then incubated with color reagents, 175 μg/ml 5-Bromo-4-chloro-3-indolyl-phosphate, 450

μg/ml 4-Nitro blue-tetrazolium chloride, and 1 mM Levamisole in NTMT for 6 h. Slides were washed with PBS containing 0.1% Tween-20, dehydrated in graded ethanols, cleared three times in xylene, and cover-slipped with Entellan. Photographs of brain sections were captured with a digital camera DP70 (Olympus, Tokyo, Japan).

Histology. Adult animals were anesthetized with Nembutal (pentobarbital sodium, 0.2 mL/100 g body weight), and fixed by transcardial perfusion with 4% paraformaldehyde in 0.1 M phosphate buffer (PB, pH 7.4). Brains were removed from the skull, embedded in paraffin. Paraffin-embedded brains were coronally sectioned at 4- or 8-μm thickness on a microtome, and mounted on APS-coated slides. For 4-μm thickness sections, every fifth sections were deparaffinized, and stained with Hematoxylin and Eosin (Merck). Stained sections were dehydrated in an ethanol series, cleaned in xylene, and then coverslipped. For 8-μm thickness, every fifth sections were also deparaffinized and stained with Bodian staining. In brief, the sections were immersed in 1% potassium dichromate for 1 h at room temperature, and then soaked in 1% silver protein (Merck) for 24 h at 37 °C. The sections were washed in the reduction solution (1 g hydroquinone, 5.6 g sodium sulphate, 140 ml distilled water) for 10 min, and then toned in 1% gold

chloride solution for 1 h. After washing, the sections were immersed in 2% oxalic acid solution for 5 min, and then soaked in 5% sodium thiosulphate solution. After rinse, the sections were dehydrated, cleared in xylene and mounted. Images were obtained with an upright light microscope equipped with a digital camera (Olympus, DP70).

Counting the number of Purkinje cells. Five micrometer coronal sections stained with Hematoxylin and Eosin were used for the quantification. The number of Purkinje cells in 6 Simple lobules was counted along 500 μm of Purkinje-cellular layer. Only the cells with a cell body in focus were counted manually. For blind analysis, name of the files were substituted with a random number.

Immunohistochemistry. Mice were anesthetized with 0.1 mg/g pentobarbital sodium and transcardially perfused with ice-cold PBS, followed by ice-cold 4% paraformaldehyde in phosphate buffer for 15 min. Olfactory mucosa and brain were dissected out and postfixed in 4% paraformaldehyde for 2 h at 4°C. Olfactory mucosa was subsequently decalcified with Morse's solution (10% w/v sodium citrate and 22.5 % v/v formic acid) for 2 days with moderate stirring at 4°C. Brain and olfactory mucosa were cryoprotected in 30% sucrose overnight at 4°C, embedded in OCT (Tissue

Tek) and frozen on powdered dry ice. Serial coronal sections at 16 μm for olfactory mucosa and at 30 μm for olfactory bulbs were made with a cryostat and collected on MAS coated slides (Matsunami) and stored at -80°C until use. Immunohistochemistry was performed as follows: sections were washed with PBS for 5 min, treated with 0.3% H_2O_2 for 30 min, rinsed in PBS for 5 min for 3 times, incubated with a blocking solution (PBS containing 5% normal horse serum and 0.3% Triton X-100) for 30 min, incubated with primary antibodies diluted in the blocking solution overnight at 4°C, washed with PBS containing 0.3% Triton X-100 (PBST) for 10 min for 3 times, incubated with biotinylated secondary antibodies diluted in blocking solution for 1 h to form immune complexes, and washed with PBST for 10 min and PBS for 10 min for 2 times. Immune complex signals were visualized using the Vectastain ABC standard kit (Vector). The primary antibodies and their dilution ratio used in this study were anti-OMP antibody, 1:2000 (Wako Chemical) and anti-Reelin antibody, 1:1000 (Calbiochem). For olfactory bulbs, antigen retrieval process was carried out by heating the sections for 40 min at 95°C in 10 mM sodium citrate (pH 6.0), kept at room temperature for 20 min and washed two times with PBS.

Methylation analysis. Genomic DNAs isolated from mouse tails were digested with either *Hpa*I alone or in combination with *Bss*HII. Southern blot analysis of differential methylation at the *Snurf-Snrpn* loci were hybridized with a 1.3-kb fragment from *Snurf* intron 1.

General health and neurological screen. A general health and neurological screen was conducted as previously described (Miyakawa *et al.*, 2001). The righting, whiskers touch, and ear twitch reflexes were evaluated, and a number of physical features including body weight and temperature, and the presence of whiskers or bald hair patches were recorded.

Neuromuscular examination. The neuromuscular strength was examined by the grip strength and wire-hanging tests. The grip strength meter (O'Hara & Co.) was used to assess forelimb grip strength. Mice were lifted and held by their tail so that their forepaws could grasp a wire grid. Mice were then gently pulled backward by the tail with their posture parallel to the surface of the table until they release the grid. The peak force applied by mouse forelimbs was recorded in Newton (Takao and Miyakawa, 2006). Each mouse was tested three times and the greatest value measured was used for

statistical analysis. In the wire hang test, mice were placed on a wire mesh, which was then inverted and waved gently, so that the subject gripped the wire. Latency to fall was recorded, with a 60 sec cut-off time.

Light/dark transition test. The apparatus used for light/dark transition test consisted of a cage (21×42×25 cm) divided into two sections of equal size by a partition with door (O'Hara & Co., Tokyo). One chamber was brightly illuminated (390 lx), whereas the other chamber was dark (2 lx). Mice were placed into the dark side, and allowed to move freely between the two chambers with door open for 10 min. The total number of transitions, time spent in each side, first latency to light side, and distance traveled were recorded automatically using Image LD software (see 'Image analysis'). On-line material describing this method is available visually (Takao and Miyakawa, 2006).

Open field test. Locomotor activity was measured using an open field test. Each subject was placed in the center of the open field apparatus (40 × 40 × 30 cm; Accuscan Instruments, Columbus, Ohio). Total distance traveled (centimeters), vertical activity (rearing measured by counting the number of photobeam interruptions), time spent in the center, the beam-break counts for stereotyped behaviors and number of fecal boli

were recorded. Data were collected for 120 min.

Hot plate test. The hot plate test was used to evaluate the nociception or the sensitivity to a painful stimulus. Mice were placed on a 55.0±0.3 ˚C hot plate (Columbus Instruments, Columbus, Ohio), and latency to the first hind-paw response was recorded. The hind-paw response was either a foot shake or a paw lick.

Social interaction test in a novel environment (one-chamber). Two mice of identical genotypes, which were previously housed in different cages, were placed into a box together (40 × 40 × 30 cm) and allowed to explore freely for 10 min. Social behavior was monitored by a CCD camera, which was connected to a Macintosh computer. Analysis was performed automatically using Image SI software. The number of contacts, the duration of contacts, and total distance traveled were measured.

Rotarod test. Motor coordination and balance were tested with the rotarod test. The rotarod test using a rotarod (UGO Basile Accelerating Rotarod) was performed by placing a mouse on a rotating drum (3 cm diameter) and measuring the time each animal was able to maintain its balance on the rod. The mouse was given two practice trials and the place on the rotating cylinder. During the trial, each mouse was placed on

the accelerated rotarod for a maximum of 300 sec, and the mean latency to fall off the rotarod (for the five trials) was recorded and used in subsequent analysis.

Startle response/prepulse inhibition tests. A startle reflex measurement system was used (O'Hara & Co., Tokyo). A test session began by placing a mouse in a plexiglas cylinder where it was left undisturbed for 10 min. The duration of white noise that was used as the startle stimulus was 40 msec for all trial types. The startle response was recorded for 140 msec (measuring the response every 1 msec) starting with the onset of the prepulse stimulus. The background noise level in each chamber was 70 dB. The peak startle amplitude recorded during the 140 msec sampling window was used as the dependent variable. A test session consisted of 6 trial types (i.e. two types for startle stimulus only trials, and four types for prepulse inhibition trials). The intensity of startle stimulus was 110 or 120 dB. The prepulse sound was presented 100 msec before the startle stimulus, and its intensity was 74 or 78 dB. Four combinations of prepulse and startle stimuli were employed (74-110, 78-110, 74-120, and 78-120). Six blocks of the 6 trial types were presented in pseudorandom order such that each trial type was presented once within a block. The average inter-trial interval was 15 sec (range: 10-20 sec).

Eight-arm radial maze test. Fully-automated eight-arm radial maze apparatuses (O'Hara & Co., Tokyo, Japan) were used. The floor of the maze was made of white plastic, and the wall (25 cm high) consisted of transparent plastic. Each arm (9 x 40 cm) radiated from an octagonal central starting platform (perimeter 12 x 8 cm) like the spokes of a wheel. Identical food wells (1.4 cm deep and 1.4 cm in diameter) with pellet sensors were placed at the distal end of each arm. The pellets sensors were able to automatically record pellet intake by the mice. The maze was elevated 75 cm above the floor and placed in a dimly-lit room with several extra-maze cues. During the experiment, the maze was maintained in a constant orientation. One week before pretraining, animals were deprived of food until their body weight was reduced to 80% to 85% of the initial level. Pretraining started on the 8th day. Each mouse was placed in the central starting platform and allowed to explore and consume food pellets scattered on the whole maze for a 30-min period (one session per mouse). After completion of the initial pretraining, mice received another pretraining to take a food pellet from each food well after being placed at the distal end of each arm. A trial was finished after the mouse consumed the pellet. This was repeated eight times, using eight different arms,

for each mouse. After these pretraining trials, actual maze acquisition trials were performed. In the spatial working memory task of the eight-arm radial maze, all eight arms were baited with food pellets. Mice were placed on the central platform and allowed to obtain all eight pellets within 25 min. A trial was terminated immediately after all eight pellets were consumed or 25 min had elapsed. An 'arm visit' was defined as traveling more than 5 cm from the central platform. The mice were confined at the center platform for 5 s after each arm choice. The animals went through one trial per day. For each trial, arm choice, latency to obtain all pellets, distance traveled, number of different arms chosen within the first eight choices, the number of arm revisited, and omission errors were automatically recorded. In the reference memory task of the eight-arm radial maze, one of the eight arms was consistently baited with one food pellet in the food well and a trial was terminated immediately after the one pellet was consumed. Data acquisition, control of guillotine doors, and data analysis were performed by Image RM software (see 'Image analysis').

Tail suspension test. The tail suspension test was performed for a 10-min test session according to toe procedures described previously (Steru et al., 1985). Mice were

suspended 30 cm above the floor in a visually isolated area by adhesive tape placed approximately 1 cm from the tip of the tail, and their behavior was recorded over a 10-min test period. Data acquisition and analysis were performed automatically, using Image TS software.

Twenty-four hour home cage monitoring. Social interaction monitoring in home cage was conducted as previously described (Miyakawa et al., 2003). To monitor social behavior between two mice in a familiar environment, a system that automatically analyzes social behavior in home cages of mice was developed. The system contains a home cage (29 x 18 x 12 cm) and a filtered cage top, separated by a 13-cm-high metal stand containing an infrared video camera, which is attached at the top of the stand. Two mice of the same inbred strain that had been housed separately were placed together in a home cage. Their social behavior was then monitored for a week. Outputs from the video cameras were fed into a Macintosh computer. Images from each cage were captured at a rate of one frame per second. Social interaction was measured by counting the number of particles in each frame: two particles indicated the mice were not in contact with each other; and one particle demonstrated contact between the two mice.

We also measured locomotor activity during these experiments by quantifying the number of pixels changed between each pair of successive frames. Analysis was performed automatically using ImageHA software (see 'Image analysis').

Contextual and cued fear conditioning. Each mouse was placed in a test chamber (26 x 34 x 29 cm) inside a sound-attenuated chamber and allowed to explore freely for 2 min. A 60 dB white noise, which served as the conditioned stimulus (CS), was presented for 30 sec, followed by a mild (2 sec, 0.5 mA) foot shock, which served as the unconditioned stimulus (US). Two more CS-US pairings were presented with 2 min inter-stimulus interval. Context testing was conducted 24 h after conditioning in the same chamber. Cued testing with altered context was conducted after conditioning using a triangular box (35 x 35 x 40 cm) made of white opaque plexiglas, which was located in a different room. Data acquisition, control of stimuli (i.e. tones and shocks), and data analysis were performed automatically, using Image FZ software. Images were captured at 1 frame per second. For each pair of successive frames, the amount of area (pixels) by which the mouse moved was measured. When this area was below a certain threshold (i.e. 20 pixels), the behavior was judged as ‘freezing’. When the amount of

area equaled or exceeded the threshold, the behavior was considered as ‘non-freezing’. The optimal threshold (amount of pixels) to judge freezing was determined by adjusting it to the amount of freezing measured by human observation. ‘Freezing’ that lasted less than the defined time threshold (i.e. 2 sec) was not included in the analysis.

Elevated plus maze Test. The elevated plus-maze consisted of two open arms (25 x 5 cm) and two enclosed arms of the same size, with 15 cm high transparent walls. The arms and central square were made of white plastic plates and were elevated to a height of 55 cm above the floor. In order to minimize the likelihood of animals falling from the apparatus, 3-mm high plexiglas ledges were provided for the open arms. Arms of the same type were arranged at opposite sides to each other. Each mouse was placed in the central square of the maze (5 x 5 cm), facing one of the closed arms. Mouse behavior was recorded during a 10-min test period. Time spent on open arms was recorded. Data acquisition and analysis were performed automatically, using Image EP software.

Porsolt forced swim test. The apparatus consisted of four plexiglas cylinders (20 cm height x 10 cm diameter). The cylinders were separated from each other by a nontransparent panel to prevent mice from seeing each other. The cylinders were filled

with water (23 ^{o}C), up to a height of 7.5 cm. Mice were placed into the cylinders, and their behavior was recorded over a 10-min test period. Data acquisition and analysis were performed automatically, using Image PS software (see Image Analysis). Immobility was measured by Image OF software (see Image Analysis) using stored image files.

Three-chambered social interaction (2). As for a novel inanimate object vs. empty, a dodecahedral pole with black and white rectangle faces alternately was used for an inanimate object and was placed in a wire cage in one side chamber. As for another inanimate object vs. a novel mouse, a black cone was used for an inanimate object and an adult conspecific mouse (C57BL/6J) that has had no previous contact with the subject (test mouse) was used for a novel mouse. As for a novel vs. familiar mouse, another adult conspecific mouse (C57BL/6J) that has had no previous contact with the subject (test mouse) was used for a novel mouse and the same mouse that was examined in the previous test was used for a familiar mouse.

Morris water task. The water maintained at room temperature (20-23 degrees) was rendered opaque by the addition of nontoxic white paint. Videotracking was conducted

with a camera focused on the full diameter of the pool. Each training trial began by placing the mouse into the quadrant that was either right of, left of, or opposite to the target quadrant containing the platform, in semirandom order. Different order of the start positions was applied every day, but the identical order of start positions was used for all subjects. Training trials were 60 s maximum duration. A mouse that failed to reach the platform within 60 s was subsequently guided to the platform. Latency to reach the platform, distance traveled to the platform, average swim speed, and percent time spent at the perimeter of the pool (thigmotaxis) were automatically recorded. Four trials per day were conducted for 4 successive days for acquisition of the visible platform task. Four trials per day were conducted for 7 successive days for acquisition of the hidden platform task with the original platform location and 4 successive days with a new platform location (reversal probe test) rotated by 180-degree from the original platform location. At the end of the seventh and eleventh days of hidden platform training, a probe test and a reversal probe test was conducted for 1 min to confirm that this spatial task was acquired based on navigation by distal environmental room cues, respectively. Time spent in each quadrant, number of crossings above the

former target site, average speed, and percent time spent at the perimeter of the pool were automatically recorded.

Barnes maze task. The circular open field was elevated 75 cm from the floor. A black Plexiglas escape box (17 × 13 × 7 cm), which had paper cage bedding on its bottom, was located under one of the holes. The hole above the escape box represented the target, analogous to the hidden platform in the Morris task. The location of the target was consistent for a given mouse but randomized across mice. The maze was rotated daily, with the spatial location of the target unchanged with respect to the distal visual room cues, to prevent a bias based on olfactory or the proximal cues within the maze. Three trials per day were conducted for 6 successive days. On day 7, a probe trial was conducted without the escape box, to confirm that this spatial task was acquired based on navigation by distal environment room cues. As for reversal task, the location of target for each mouse was shifted to the complete opposite side on circular surface. Same trials were also carried out and conducted a probe trial. Time spent around each hole was recorded by videotracking software (Image BM).

T-maze test. Left-right discrimination task was conducted using an automatic T-maze

(Tujimura et al., 2008). It was constructed of white plastics runways with walls 25-cm high. The maze was partitioned off into 6 areas by sliding doors that can be opened downward. The stem of T was composed of area S2 (13 × 24 cm) and the arms of T were composed of area A1 and A2 (11.5 × 20.5 cm). Area P1 and P2 were the connecting passage way from the arm (area A1 or A2) to the start compartment (area S1). The end of each arm was equipped with a pellet dispenser that could provide food reward. The pellet sensors were able to record automatically pellet intake by the mice. One week before the pre-training, mice were deprived of food until their body weight was reduced to 80-85% of the initial level. Mice were kept on a maintenance diet throughout the course of all the T-maze experiments. Before the first trial, mice were subjected to three 10-min adaptation sessions, during which they were allowed to freely explore the T-maze with all doors open and both arms baited with food. On the day after the adaptation session, mice were subjected to a left-right discrimination task for 6 days (one session consisting of 10 trials, 2 sessions per day; cutoff time, 50 min). Mice were given 10 pairs of training trials per day. The mouse was able to freely choose either the right or left arm of the T (area A1 or A2). Correct arm was assigned to each mouse

randomly. If a mouse chose the correct arm, mouse could receive a reward at the end of the arm. Choosing an incorrect arm resulted in no reward and confinement to the arm for 10 sec. After the mouse consumed the pellet or the mouse stayed more than 10 sec without consuming the pellet, door that separated the arm (area A1 or A2) and connecting passage way (area P1 or P2) would be opened and the mouse could return to the starting compartment (area S1), via connecting passage way. On the 7th day, the correct arm was changed to the opposite for reversal learning. A variety of fixed extra-maze clues surrounded the apparatus.

Image analysis. All applications used for the behavioral studies (Image EP, Image BM, Image SI and Image PS) were run on a Macintosh computer. Applications were based on the public domain NIH Image or Image J program (developed by Wayne Rasband at the U.S. National Institute of Mental Health and available on the Internet at http://rsb.info.nih.gov/nih-image/) and were modified for each test by Tsuyoshi Miyakawa (available through O'Hara & Co.).

Ultrasonic vocalization. Both male and female pups (P5–22) were used. Pups were raised with their mother and littermates in a cage placed in an animal holding room

(room temperature: 23.0 ± 2.0 ºC, humidity: 55.0 ± 15.0%) with a 12 h light-dark cycle (lights on at 07:00). On the day of the study, the pups with their mother were moved to the experimental room at least 60 min before the initiation of the study. After habituation, each pup was removed from its mother and placed in a stainless-steel cylinder (size 7.5 cm diameter x 7 cm height) on the COOL PLATE® (NCP-2215, Nisshin Rika Co., Ltd.) which maintained temperature of the cylinder at 24 ºC in a sound proof room (AT-81, RION Co., Ltd.). The number of vocalization was measured for 5 min. Individual calls made by each pup were collected by an ultrasound detectable microphone (UC-29, RION Co., Ltd.), and them amplified by a preamplifier (NH-05A, RION Co., Ltd.) and a main amplifier (UN-04A, RION Co., Ltd.) with a filter (Multifunction filter 3611, NF Corporation Co., Ltd., settings: high pass 1.5 kHz). Then analog signals were converted to digital signals by an A/D converter (CH-3150, Exacq Technologies, Inc.), and stored in a personal computer (PRECISION 470®, Dell Inc.). The numbers of vocalizations were counted by the recording software (Dasy Lab® 9.0, measX GmbH and Co. KG.) with a digital filter at 20 kHz to count the vocalizations generated at ultrasound range. The threshold value was set at a signal amplitude of 0.05

V to exclude noise. Measurements of vocalizations were conducted at 5, 7, 14 days and 3 weeks (21 or 22 days) after the birth. Each pup was immediately returned to its mother in the home cage after the measurement. Surface body temperature of each pup was monitored with an infrared thermometer (Thermo-Hunter PT3S, Optex Co., Ltd.) immediately before and after the isolation. In the case of power spectrum analysis, stored signals were transformed with the fast Fourier transformation method by the software.

Vocalization in a resident-intruder paradigm. Male mice (14 WT and 14 *patDp/+* mice, 7-8 weeks) were used. Resident mice were individually housed for 4 weeks before the test session. Intruder mice were maintained in social groups of three to four per home cage for 1 week before the test session. Body weights of resident and intruder mice were comparable (WT: resident vs. intruder; 20.6 +/- 0.5 g vs. 21.4 +/- 0.4 g, *patDp/+*: resident vs. intruder; 22.8 +/- 0.5 g vs. 21.8 +/- 1.0 g). On the day of the study, the animals were moved to the experimental room from the animal room and left for at least 60 min before initiation of the study. After habituation, the cage with a resident mouse was placed under an ultrasound detectable microphone in a sound proof room.

Both audible (frequency between 1.5 kHz and 20 kHz) and ultrasonic (above 20 kHz) vocalizations were recorded with the same system for maternal separation study except using both 1.5kHz and 20 kHz filters to separate ultrasonic calls from total calls, because an adult mouse emitted calls ranging from audible to ultrasonic bands. A pair of resident and intruder mice was made from the same genotyped mice. An intruder was introduced into the home cage of a resident mouse for 10 min. Total calls emitted by a pair of resident and intruder mice for the last 5 min were recorded. Resident showed agonistic behavior against intruder in the first 5 min, thus vocalization during this period may be affected by the high level of emotion. After measurement, an intruder mouse was removed from the home cage of a resident mouse. The test was conducted between 13:00 and 17:00.

Olfactory habituation/dishabituation test. The ability of the mice to detect social and non-social odors was examined with the olfactory habituation/dishabituation method as previously described (Crawley et al., 2007) with some modifications. The animal was transferred to the testing room and reared individually 6 h prior to testing. One hour before the test, for acclimatizing the swab itself, swab was adhered with the tape on

each cage lid where mice could not contact directly because of the existence of wire bars of lid between them. The swab tip was placed at a level 5 cm from the bottom of the cage. All testings were done in the light, but during the dark phase of the light cycle. During the test, food and water were deprived and lid was changed to a clean one. Odorant stimuli were ultrapure water, cage of female mice, banana extract (Golden Kelly Patent Flavor Co, Ltd., Osaka, Japan) diluted 1:10 in ultrapure water, and almond extract (Golden Kelly Patent Flavor Co, Ltd.) diluted 1:10 in ultrapure water. The choice of these odorants and dilutions was based on data from pilot experiments in our laboratory. Experimenters prepared stimuli by dipping a swab into the stimulus solution (water, banana, and almond) or by wiping in a zig-zag pattern across the floor of the dirty cage of female mice by the water-soaked swab. The swab was consequently adhered by the tape on the cage lid at a level 5 cm from the bottom of the cage. Each stimulus was presented for 2 min and then replaced by a new applicator, three times in succession for a total of 12 presentations. The order of presentation was water, cage, banana and almond. The behavior was monitored by an 8-mm video camera and was recorded on a PC. By using the recorded data, the amount of time the subject spent with

its nose above the wire bars beneath the swab was counted by stopwatch later.

RNA blot hybridization. RNAs were isolated from mouse brains by SV total RNA isolation system (Promega). One μg of total RNA was electrophoresed on a 1% formaldehyde gel and transferred to a Hybond-N+ membrane (Amersham). The membrane was hybridized with γ^{32}P-ATP labeled MBII52 probe (72-bp) and α^{32}P-dCTP labeled G3PDH probe at 65 ^{o}C. The filter was washed in 0.6x SSC and 1% SDS at 65 ^{o}C. BAS-2000 (Fuji Photo Film) was used for imaging and its quantification.

Pyrosequencing. The pyrosequencing analysis was conducted according to the previous report (Iwamoto et al., 2005). Four μl of streptavidin-sepharose beads (Amersham) and 29 μl of binding buffer (10 mM Tris-HCl, 1 mM EDTA, 2 M NaCl, 0.1% Tween 20 at pH 7.6) were mixed with 25 μl of RT-PCR product for 10 min at room temperature. The reaction mixture was placed onto a MultiScreen-HV, Clear Plate (Millipore). After applying the vacuum, the beads were treated with a denaturation solution (0.2 N NaOH) for 1 min, and washed twice with washing buffer (10 mM Tris-Acetate at pH 7.6). The beads were then suspended in 50 μl of annealing buffer (20 mM Tris-Acetate, 2 mM Mg-Acetate at pH 7.6) containing 10 pmol of sequencing

primer. The template-sequencing primer mixture was transferred onto a PSQ 96 Plate (Biotage), heated to 90 ^{o}C for 2 min, and cooled to room temperature. Sequencing reactions were performed with a PSQ 96 SNP Reagent Kit (Biotage) using a PSQ96MA (Biotage) according to the manufacture's instructions.

References

Crawley, J.N., Chen, T., Puri, A., Washburn, R., Sullivan, T.L., Hill, J.M., Young, N.B., Nadler, J.J., Moy, S.S., Young, L.J.*, et al.* (2007). Social approach behaviors in oxytocin knockout mice: comparison of two independent lines tested in different laboratory environments. Neuropeptides *41*, 145-163.

Inoue, K., Terashima, T., Nishikawa, T., and Takumi, T. (2004). Fez1 is layer-specifically expressed in the adult mouse neocortex. Eur J Neurosci *20*, 2909-2916.

Iwamoto, K., Bundo, M., and Kato, T. (2005). Estimating RNA editing efficiency of five editing sites in the serotonin 2C receptor by pyrosequencing. Rna *11*, 1596-1603.

Miyakawa, T., Leiter, L.M., Gerber, D.J., Gainetdinov, R.R., Sotnikova, T.D., Zeng, H., Caron, M.G., and Tonegawa, S. (2003). Conditional calcineurin knockout mice exhibit multiple abnormal behaviors related to schizophrenia. Proc Natl Acad Sci U S A *100*, 8987-8992.

Miyakawa, T., Yamada, M., Duttaroy, A., and Wess, J. (2001). Hyperactivity and intact hippocampus-dependent learning in mice lacking the M1 muscarinic acetylcholine

receptor. J Neurosci *21*, 5239-5250.

Robertson, E.J. (1987). Embryo-derived stem cell lines. In Teratocarcinomas and embryonic stem cells: A practical approach, E.J. Robertson, ed. (Oxford, IRL Press), pp. 71-112.

Steru, L., Chermat, R., Thierry, B., and Simon, P. (1985). The tail suspension test: a new method for screening antidepressants in mice. Psychopharmacology (Berl) *85*, 367-370.

Takao, K., and Miyakawa, T. (2006). Light/dark transition test for mice. J Vis Exp, 104.

Tujimura, A., Matsuki, M., Takao, K., Yamanishi, K., Miyakawa, T., and Hashimoto-Gotoh, T. (2008). Mice lacking the kf-1 gene exhibit increased anxiety- but not despair-like behavior. Front Behav Neurosci.

Legends for supplemental figures

Figure S1. Histology of the adult mouse brain analysed by HE staining. (**A** to **C**) Olfactory bulb (Ob), Scale bar, 200 μm. (**D** to **F**) Cortex (Ctx), Scale bar, 500 μm. The numbers of cortical cells in a 1.7 mm x 1.28 mm area of the retrosplenial cortex did not show any significant difference between *patDp*/+, *matDp*/+ and WT mice. (**G** to **I**) Hippocampus (Hp), Scale bar, 500 μm. (**J to L**) Amygdala (Amg), Scale bar, 1 mm. (**M** to **O**) Cerebellum (Cb), Scale bar, 1 mm. (**P** to **R**) Cb (Purkinje). Scale bar, 100 μm.

Figure S2. The number of Purkinje cells in the cerebellum. The number of Purkinje cells in the cerebellar simple lobule was counted along a 500 μm length of the Purkinje-cell layer. P14 (n=3) and adult (n=3) mice were used. (**A**) In wild type mice, the number of cells at P14 was significantly greater compared with the adult mice. *, $p<0.05$; t-test. However, there was no significant difference in *pat*Dp/+ mice. (**B**) No significant difference between the two genotypes both at P14 and in the adult. Error bars indicate SEM (standard error of the mean).

Figure S3. mRNA expression in mouse peripheral tissues analysed by quantitative RT-PCR. The expression levels of *patDp*/+ (n=3) and *matDp*/+ (n=3) were compared with that of WT (n=3), which was defined as 1.0. *Tubgcp5* is a control gene that is located outside the duplicated region. Error bars, SEM. *, $p<0.05$.

Figure S4. *patDp/*+ (129SvEv) mice have decreased sociability. Three-chamber test, (**A**) Schematic representaion of the 3-chambered apparatus. S and E represent the stranger mouse and empty, respectively. The quadrant spaces depicted by the dotted lines were used for quantitative analysis. Average image for all traces of WT (upper **B**, n=22) and *patDp*/+ mice (upper **C**, n=21). Comparison of time spent in the quadrant spaces between S and E for WT mice (lower **B**) and *patDp*/+ (lower **C**). Error bars, SEM. **, $p<0.01$. A stranger mouse is restricted in one of the side chambers in a wire cage (depicted as S), and the opposite chamber is left empty (E). Images of movement traces for 10 min (WT; n=22, *patDp/*+; n=21) are shown in B and C with the warmer colors representing more time spent in that particular location. (**B**) WT mice tended to contact the stranger mouse (arrow) and the time spent with the stranger mouse in the

quadrant location depicted by the dotted line in A was significantly higher than that in the opposite empty chamber. (**C**) In contrast, the *patDp/+* mice tended to stay more in the central chamber, preferably in the corners. Some stayed longer at the edges (arrow). Thus, no significant difference in time spent between the quadrant spaces of either side was observed.

Figure S5. *patDp/+* mice show decreased sociability. (**A**) A novel object (a dodecahedral pole) is placed in a cage in the chamber on one side and no object in the chamber on the other side. Both WT and *patDp/+* mice showed more number of entries around the cage with a novel object. **, $p<0.001$. (**B**) Another novel object (a cone) is placed in a cage in the chamber on one side and an adult conspecific mouse (C57BL/6J) that has had no previous contact with the subject (test mouse) is placed in a cage in the chamber on the other side. (**C**) A novel stranger mouse (C57BL/6J) is placed in a cage in the chamber on one side and a familiar mouse that has been used in a previous test in B is placed in the chamber on the other side. n=11. *, $p=0.05$. These data were evaluated by *t*-test.

Figure S6. *matDp*/+ mice do not show any significantly different behavior compared with WT in the three-chamber test. Average image for all traces of WT (upper A, n=18) and *matDp*/+ mice (upper B, n=18). Comparison of time spent in quadrant spaces between S and E in WT (lower A) and *matDp*/+ mice (lower B). Error bars, SEM. **, $p<0.01$. *, $p<0.05$.

Figure S7. Behavioral inflexibility of *patDp/+* mice. Barnes maze test, n=21; *patDp*/+, n=22; WT. (**A**) The hole at 0 degrees is the correct hole chosen as the target. **(B)** The reversal learning task of the Barnes maze. Error bars, SEM. *, $p<0.05$.

Figure S8. *matDp*/+ mice do not show any significantly different behavior compared with WT in the Barnes maze test and USVs. (**A**) Barnes maze test, n=17; *matDp*/+ mice, n=17; WT mice. (**B**) The reversal learning task of the Barnes maze. Error bars, SEM. (**C**) Maternal separation-induced ultrasonic vocalizations at P5, 7, 14, and 21 (or 22). n=13, 17, 17, and 9; *matDp*/+ mice, n=16, 25, 25, and 12; WT mice.

Error bars, SEM.

Figure S9. Changes in USV frequency distribution during postnatal periods in mouse pups with the duplication. When the power spectrum of vocalization frequency was generated, a digital filter at 20 kHz was disengaged.

Figure S10. Adult *patDp/+* mice exhibit decreased vocalization in the resident-intruder test. (**left**) Total vocalization ranging from audible to ultrasonic bands during the last 5 min in a 10 min resident-intruder paradigm. (**right**) Ultrasonic vocalizations during the last 5 min in a 10 min resident-intruder paradigm. Seven pairs were analyzed for both WT and *patDp/+* mice. One-tailed Mann-Whitney U test was used to compare the difference in the number of vocalizations between WT and *patDp/+* mice. * $p<0.05$

Figure S11. *patDp/+* mice show anxiety. (**A** to **C**) Cued and contextual conditioning test. No significant difference between *patDp*/+ and WT mice during conditioning

training (**A**) or in the same contextual condition (**B**). n=22 both for *patDp*/+ and WT mice. In the altered contextual environment (**C**), *patDp*/+ mice exhibited higher freezing scores during the first 3 minutes in the absence of the cue compared with WT. Error bars, SEM. *, $p<0.05$. (**D** to **G**) Elevated plus maze test. n=22 both for *patDp*/+ and WT mice. No significant difference in traveled distance between *patDp*/+ and WT mice (**D**). The number of entries (**E**) and time on the open arms (**F**) for *patDp*/+ mice were significantly decreased compared with those for WT. Error bars, SEM. *, $p<0.05$. (**G**) There was no significant difference in entries into the closed arm between *patDp*/+ and WT mice.

Figure S12. *matDp*/+ mice do not show anxiety. (**A** to **C**) Cued and contextual conditioning test. n=18; *matDp*/+ mice, n=18; WT mice. There was no significant difference between *matDp*/+ and WT mice during conditioning training (**A**), in the same contextual condition (**B**) and in the altered contextual environment in the presence of the cue (**C**). Error bars, SEM. (**D** to **G**) Elevated plus maze test. n=18; *matDp*/+ mice, n=18; WT mice. There was no significant difference in traveled distance (**D**), the

number of entries (**E**), time on open arms (**F**) entries into the closed arms (**G**) between *matDp*/+ and WT mice. Error bars, SEM.

Figure S13. RNA editing sites on the 5-HT2cR and editing ratios. Five boxed sites of adenine (A-E), their possible triplet codes (amino acids), and their encoded amino acid numbers (157, 159 and 161) are shown in the upper portion. Error bars, SEM. n=4; *patDp*/+ mice, n=5; *matDp*/+ mice, n=7; WT mice. **, $p<0.01$, *, $p<0.05$.

Figure S14. Rotarod performance of *patDp*/+ mice. *patDp*/+ mice showed a significantly greater improvement in rotarod performance compared with WT mice. n=21; *patDp*/+ mice, n=22; WT mice. Error bars, SEM. **, $p<0.01$.

Figure S15. *patDp*/+ mice show anxiety. Porsolt forced swim task. *patDp*/+ mice showed higher levels of immobility compared with WT mice both at Day 1 and Day 2. Error bars, SEM. n=22; *patDp*/+ mice, n=22; WT mice. *, $p<0.05$, **, $p<0.01$.

Table S1. A list of behavioral tests performed (WT vs. *patDp*/+ mice)

Table S2. A list of behavioral tests performed (WT vs. *matDP/+* mice)

Fig. S1

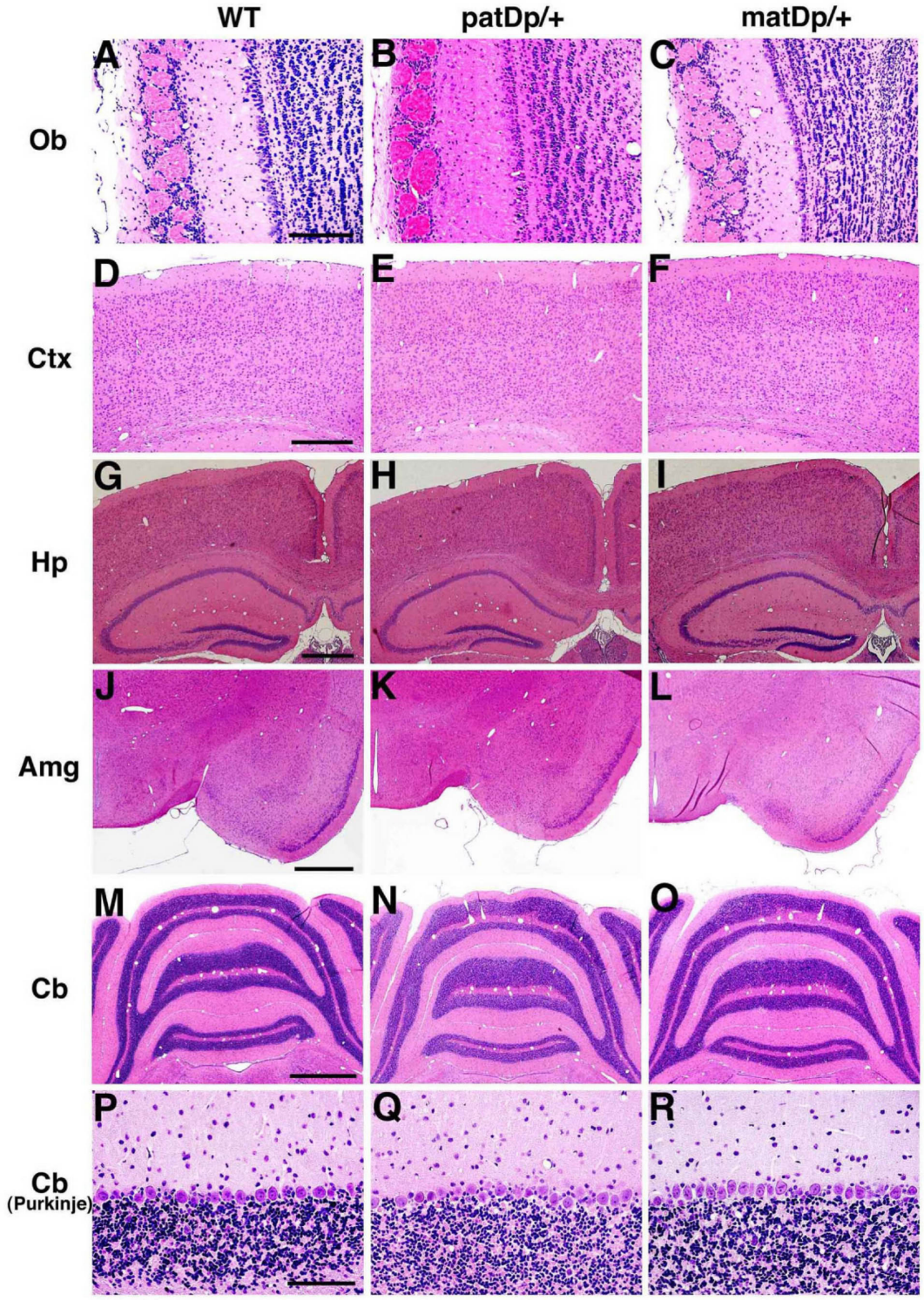
WT
patDp/+
matDp/+
Ob
Ctx
Hp
Amg
Cb
Cb
(Purkinje)
A
B
C
D
E
F
G
H
I
J
K
L
M
N
O
P
Q
R

Fig. S2

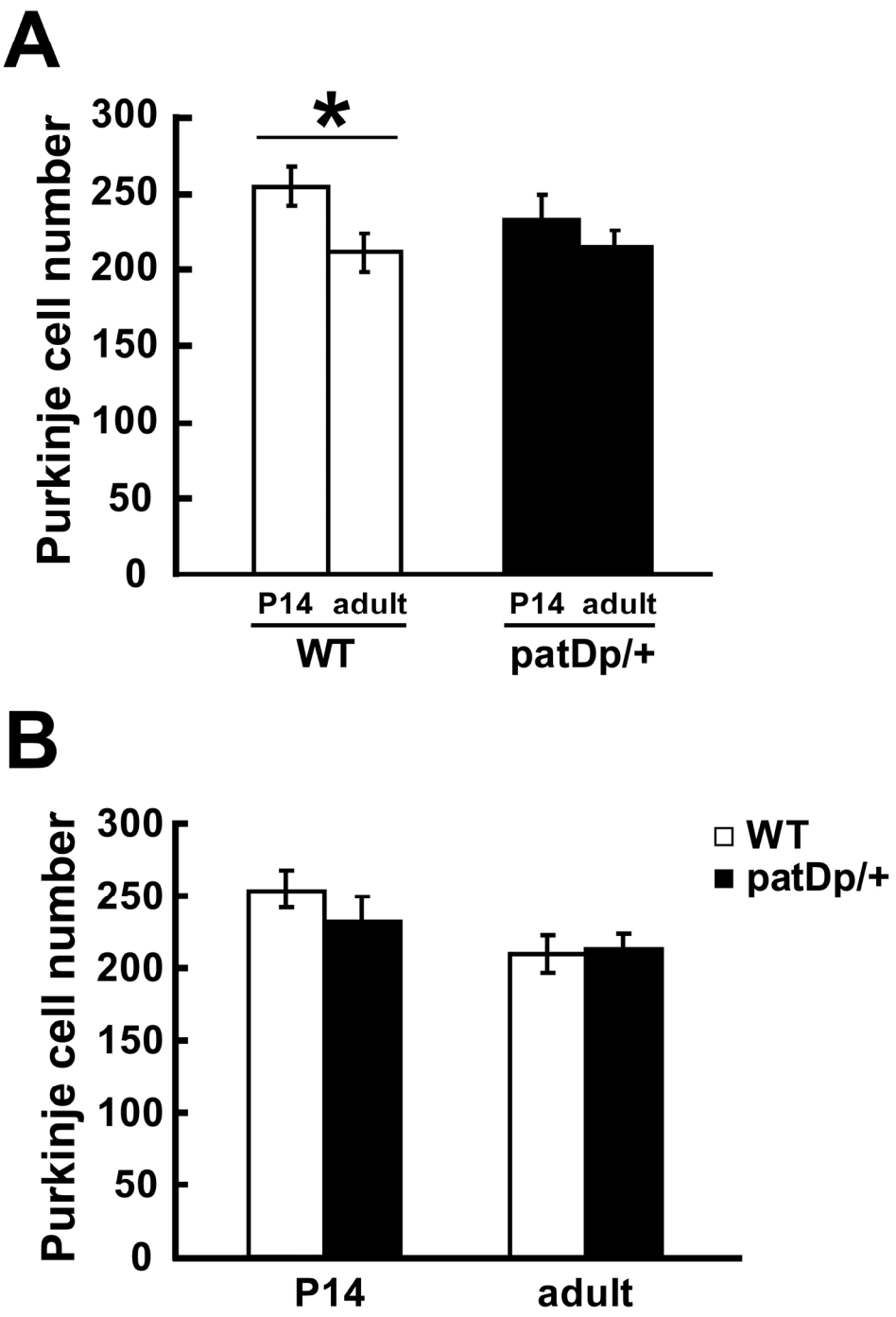
A
Purkinje cell number
300
250
200
150
100
50
0
*
P14
adult
WT
P14
adult
patDp/+
B
Purkinje cell number
300
250
200
150
100
50
0
WT
patDp/+
P14
adult

Fig. S3

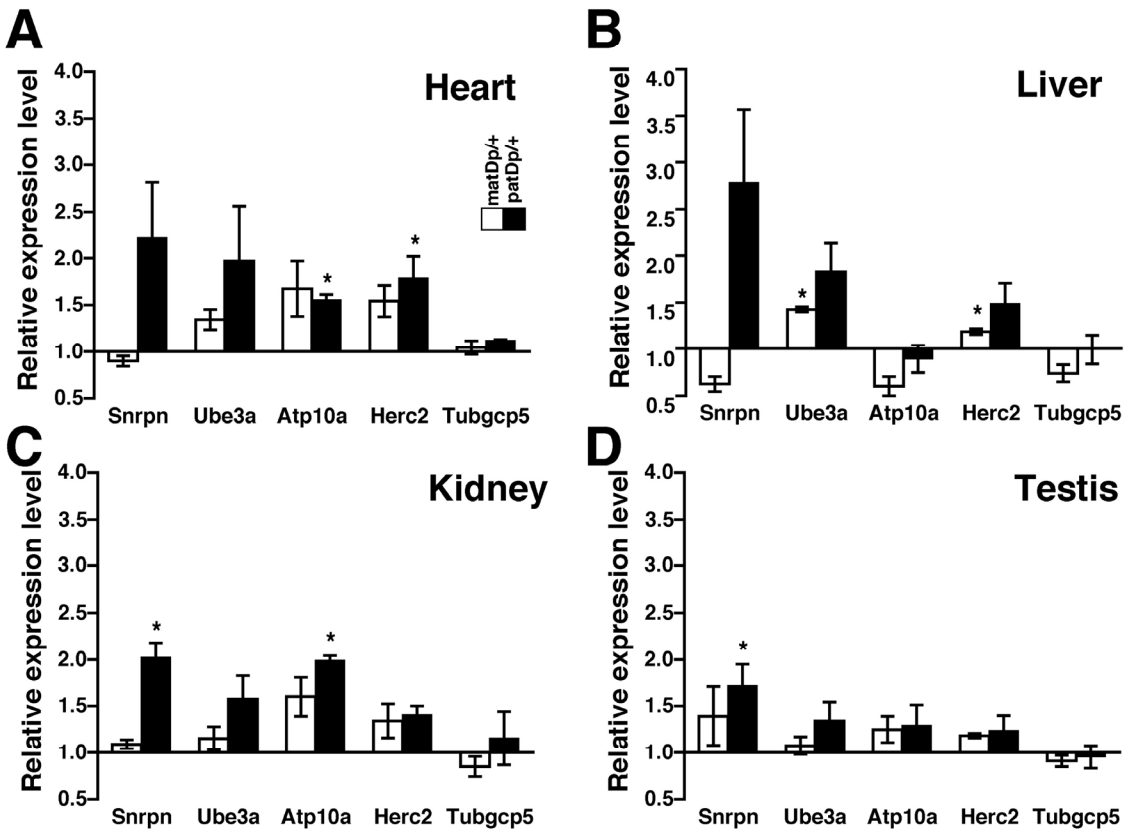
A
Heart
matDp/+
patDp/+
Relative expression level
4.0
3.5
3.0
2.5
2.0
1.5
1.0
0.5
Snrpn
Ube3a
Atp10a
Herc2
Tubgcp5
B
Liver
C
Kidney
D
Testis

Fig. S4

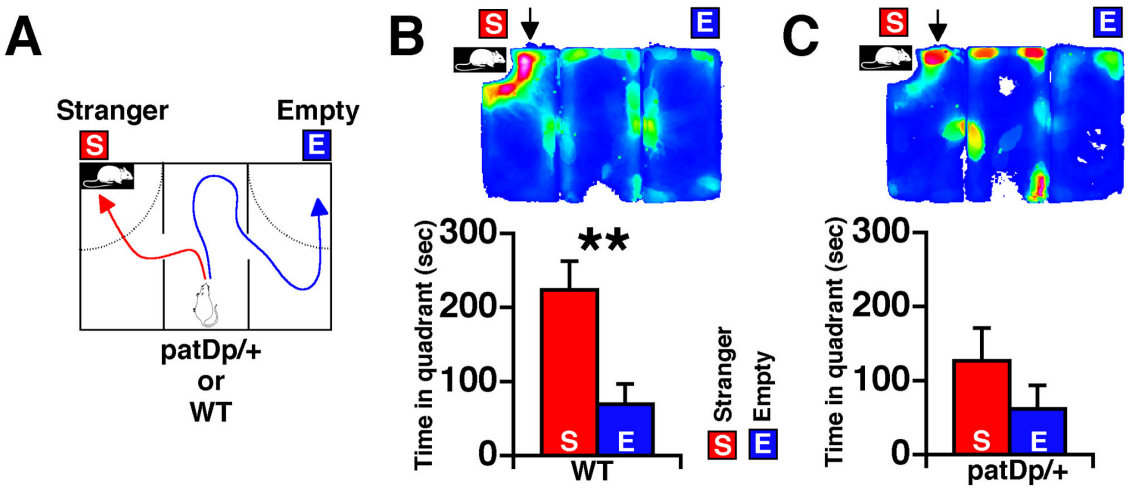
A
Stranger
Empty
S
E
patDp/+
or
WT
B
S
E
Time in quadrant (sec)
300
200
100
0
**
S
E
WT
Stranger
Empty
S
E
C
S
E
Time in quadrant (sec)
300
200
100
0
S
E
patDp/+

Fig. S5

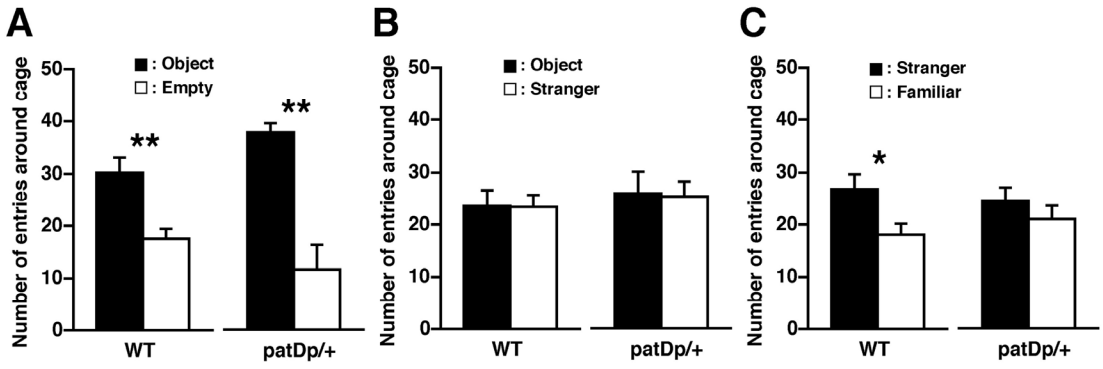
A
B
C
Number of entries around cage
■ : Object
□ : Empty
■ : Object
□ : Stranger
■ : Stranger
□ : Familiar
0
10
20
30
40
50
**
**
*
WT
patDp/+

Fig. S6

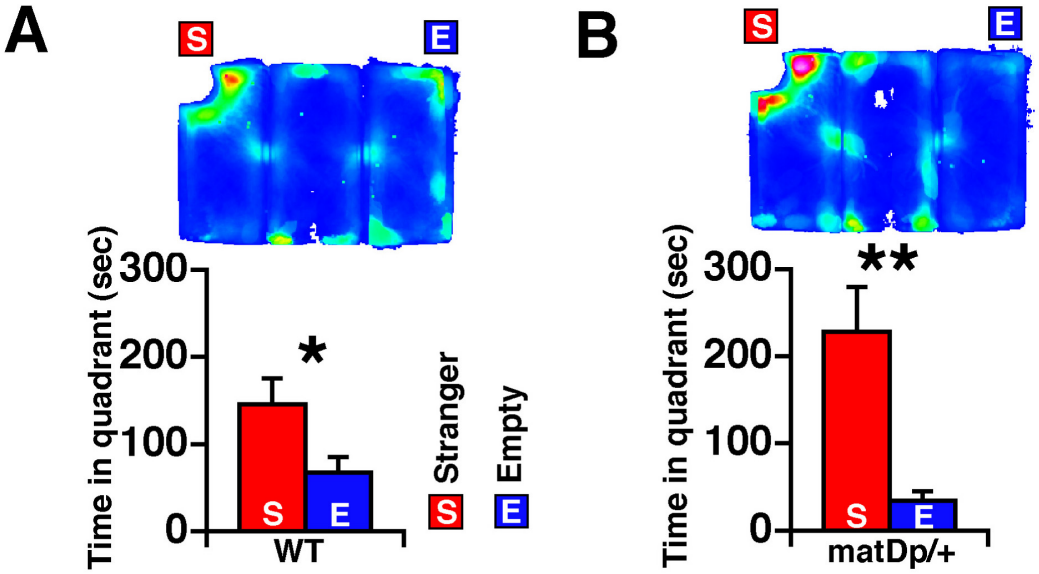
A
S
E
Time in quadrant (sec)
300
200
100
0
*
S
E
WT
Stranger
S
Empty
E
B
S
E
Time in quadrant (sec)
300
200
100
0
**
S
E
matDp/+

Fig. S7

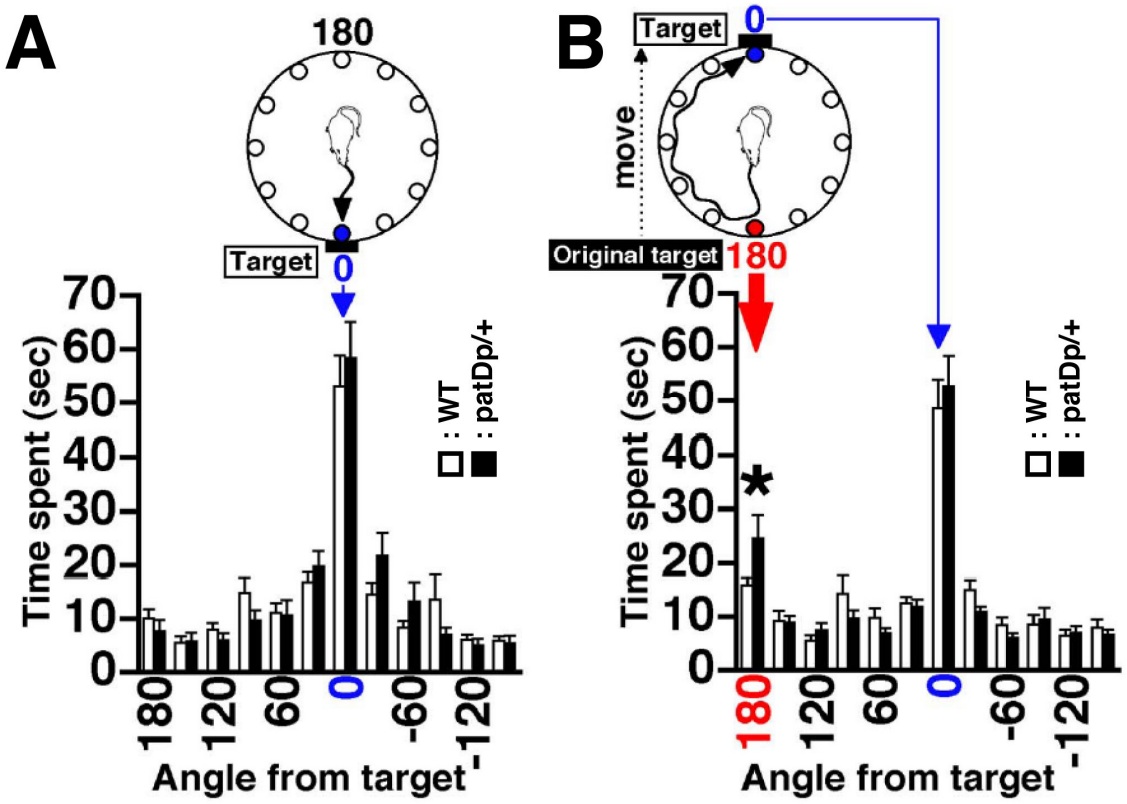
A
180
Target
0
Time spent (sec)
70
60
50
40
30
20
10
0
180
120
60
0
-60
-120
Angle from target
□ : WT
■ : patDp/+
B
Target
0
move
Original target
180
*
Time spent (sec)
Angle from target
□ : WT
■ : patDp/+

Fig. S8

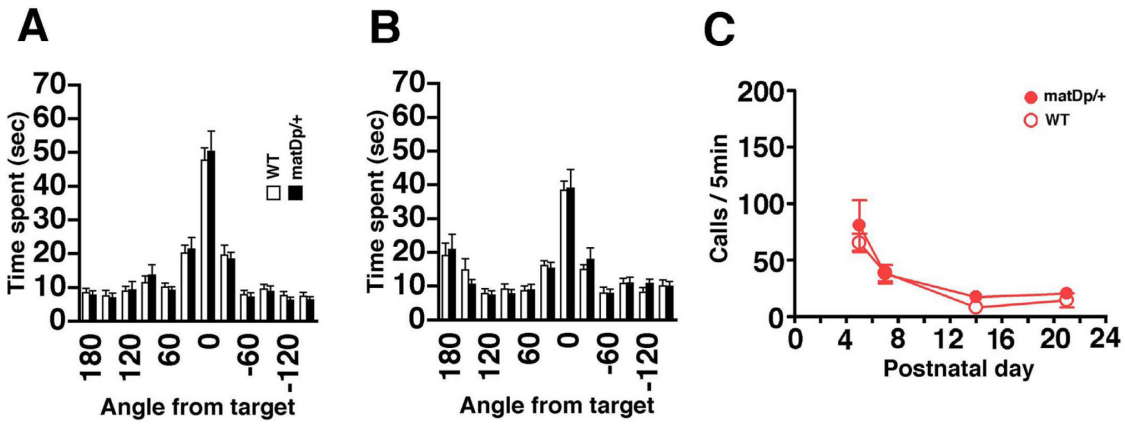
A
B
C
Time spent (sec)
70
60
50
40
30
20
10
0
180
120
60
0
-60
-120
Angle from target
WT
matDp/+
Calls / 5min
200
150
100
50
0
4
8
12
16
20
24
Postnatal day

Fig. S9

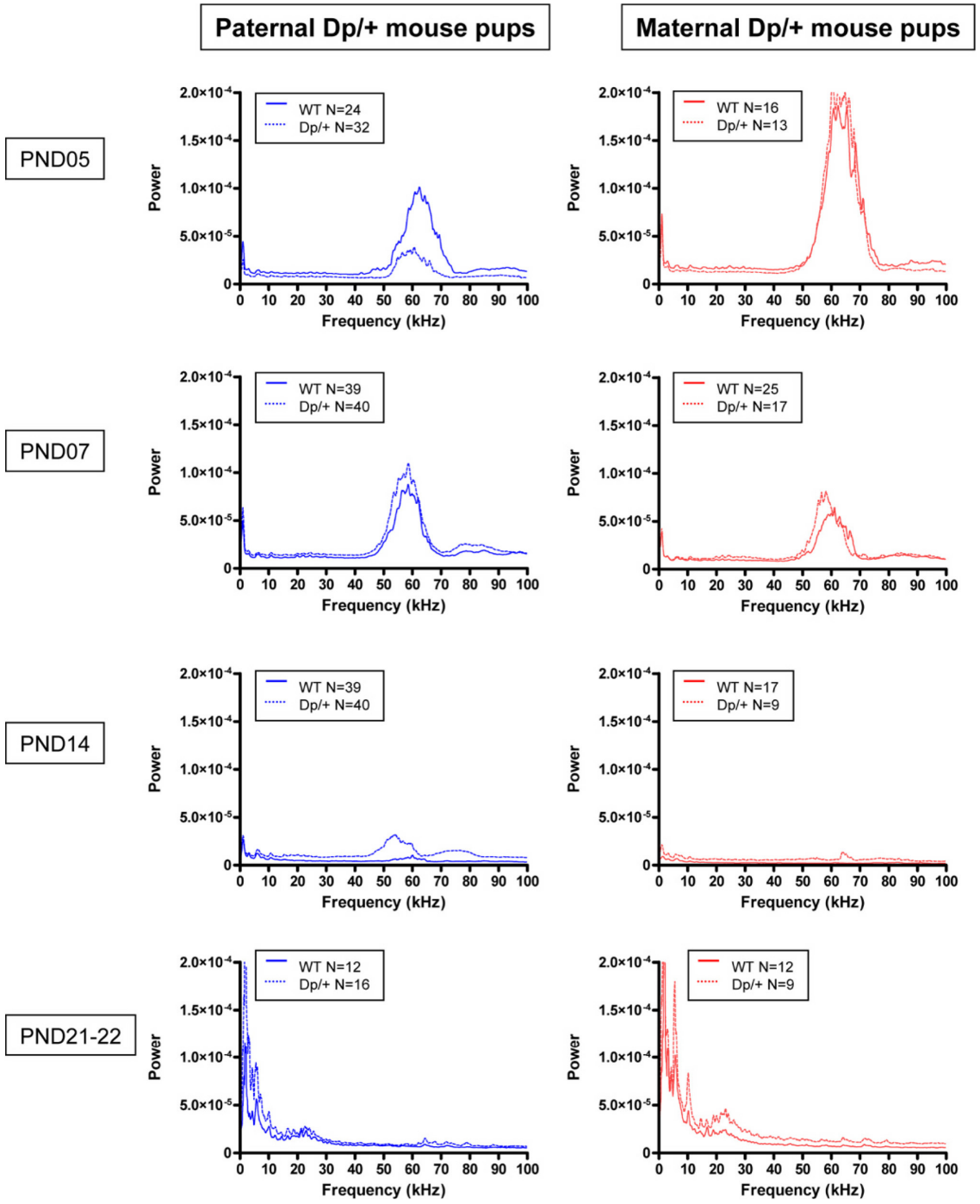
Paternal Dp/+ mouse pups
Maternal Dp/+ mouse pups
PND05
PND07
PND14
PND21-22
WT N=24
Dp/+ N=32
WT N=16
Dp/+ N=13
WT N=39
Dp/+ N=40
WT N=25
Dp/+ N=17
WT N=39
Dp/+ N=40
WT N=17
Dp/+ N=9
WT N=12
Dp/+ N=16
WT N=12
Dp/+ N=9
Power
Frequency (kHz)

Fig. S10

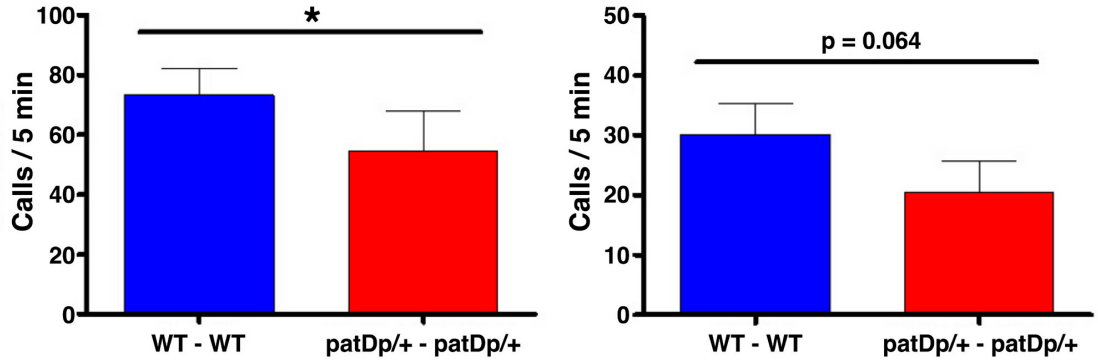
100
80
60
40
20
0
Calls / 5 min
*
WT - WT
patDp/+ - patDp/+
50
40
30
20
10
0
Calls / 5 min
p = 0.064
WT - WT
patDp/+ - patDp/+

Fig. S11

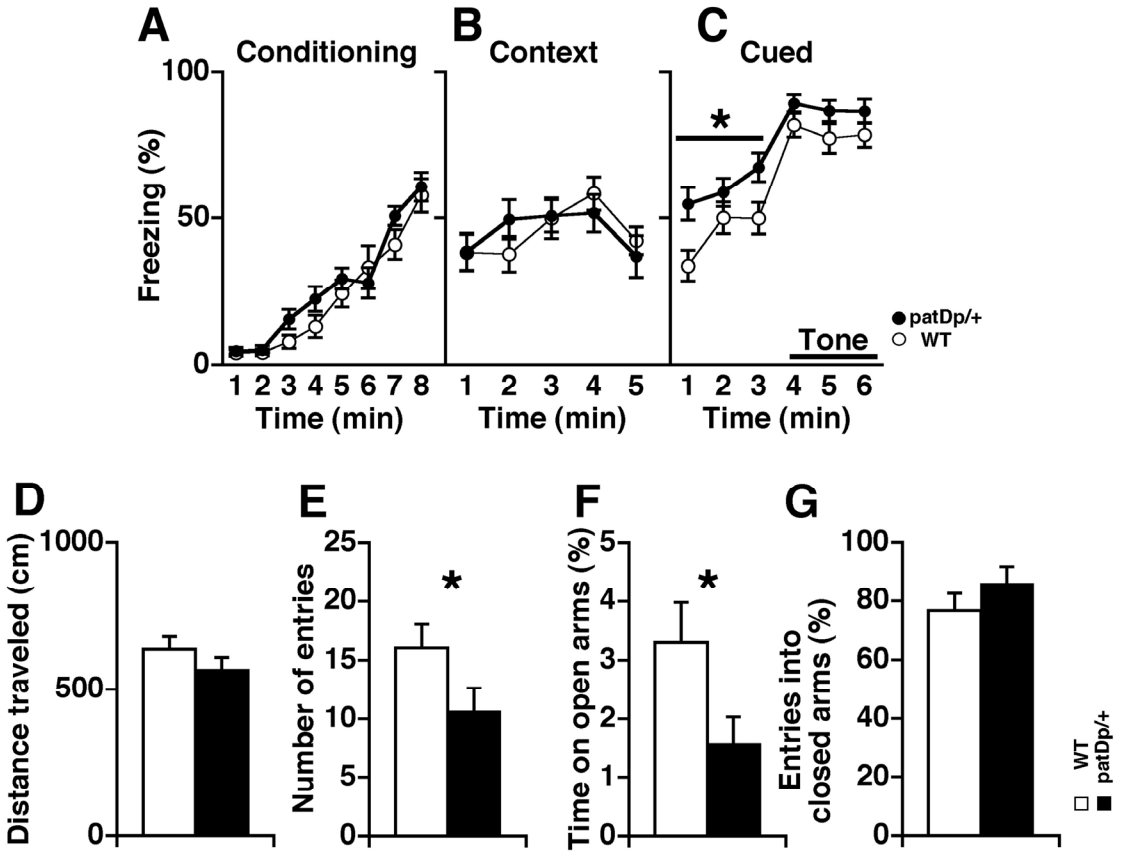
A
Conditioning
B
Context
C
Cued
Freezing (%)
100
50
0
1 2 3 4 5 6 7 8
1 2 3 4 5
1 2 3 4 5 6
Time (min)
Time (min)
Time (min)
*
Tone
patDp/+
WT
D
Distance traveled (cm)
1000
500
0
E
Number of entries
25
20
15
10
5
0
*
F
Time on open arms (%)
5
4
3
2
1
0
*
G
Entries into closed arms (%)
100
80
60
40
20
0
WT
patDp/+

Fig. S12

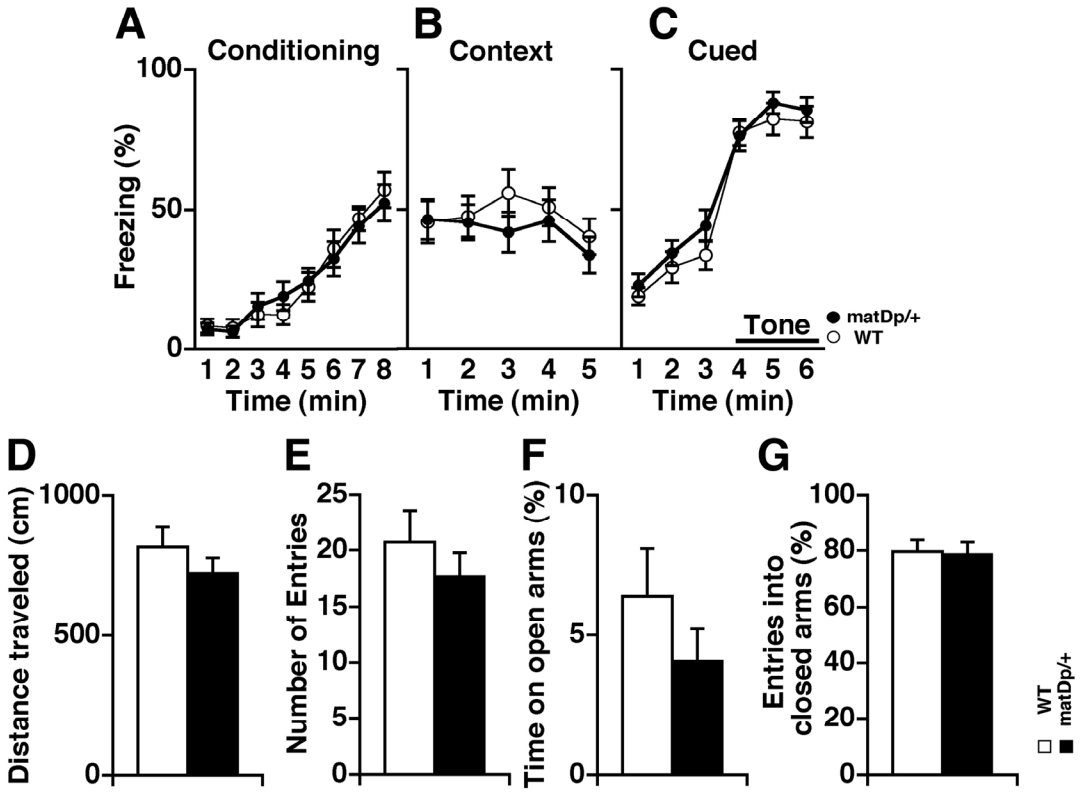
A
Conditioning
B
Context
C
Cued
Freezing (%)
100
50
0
1 2 3 4 5 6 7 8
1 2 3 4 5
1 2 3 4 5 6
Time (min)
Time (min)
Time (min)
Tone
matDp/+
WT
D
Distance traveled (cm)
1000
500
0
E
Number of Entries
25
20
15
10
5
0
F
Time on open arms (%)
10
5
0
G
Entries into closed arms (%)
100
80
60
40
20
0
WT
matDp/+

Fig. S13

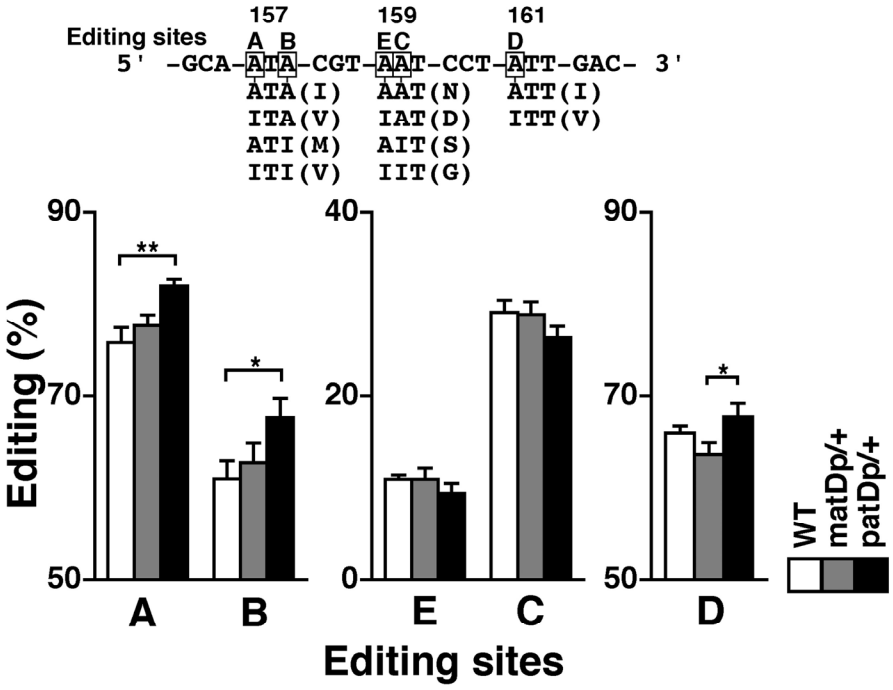
157
159
161
Editing sites
A B
EC
D
5' -GCA-ATA-CGT-AAT-CCT-ATT-GAC- 3'
ATA(I)
AAT(N)
ATT(I)
ITA(V)
IAT(D)
ITT(V)
ATI(M)
AIT(S)
ITI(V)
IIT(G)
Editing (%)
90
70
50
40
20
0
**
*
*
A
B
E
C
D
Editing sites
WT
matDp/+
patDp/+

Fig. S14

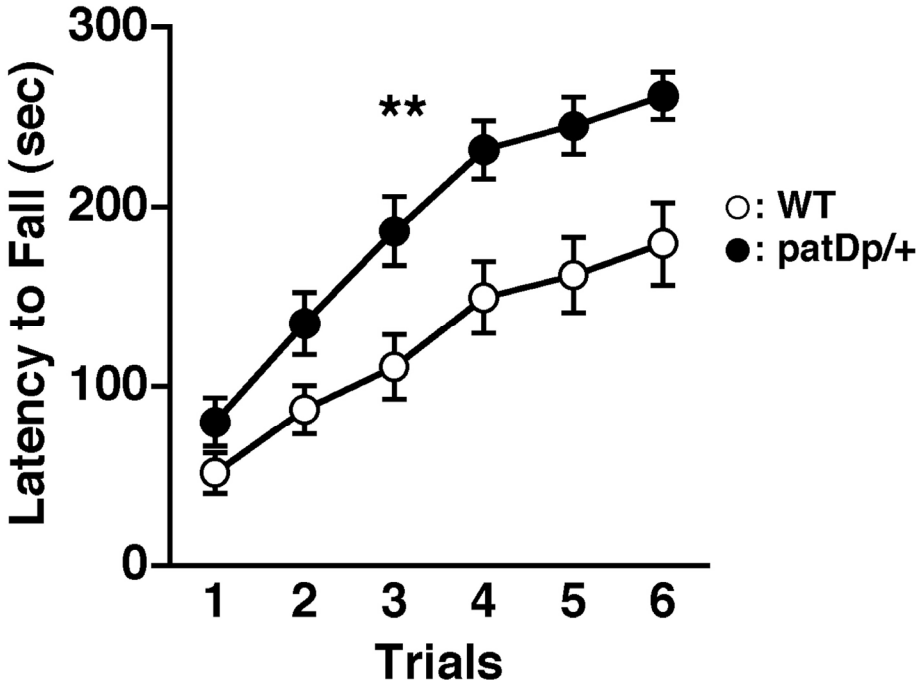

Fig. S15

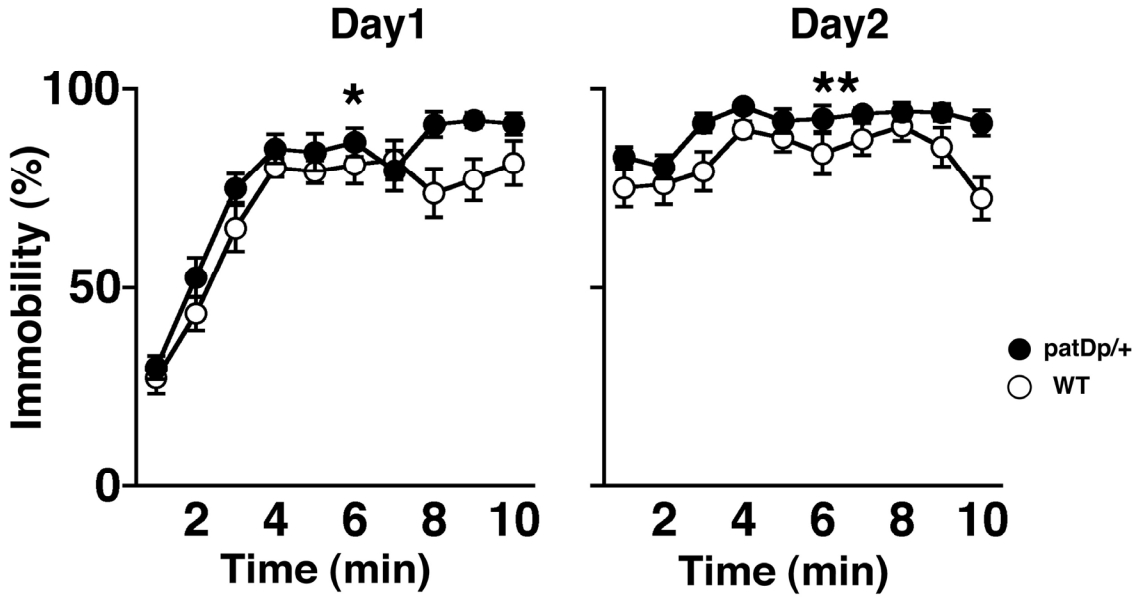
Day1
Day2
100
50
0
Immobility (%)
*
**
2 4 6 8 10
Time (min)
2 4 6 8 10
Time (min)
patDp/+
WT

Table S1

Supplemental Table 1
A list of behavioral tests in 129 strain (WT vs patDp/+)

Behavioral test			Mean ± SEM		*F* value	*P* value [a]
			WT	patDp/+		
General health	Weight (g)		25.309 ± 0.521	25.382 ± 0.588	F(1,42)=0.009	0.9267
	Temperature (℃)		36.614 ± 0.153	36.382 ± 0.123	F(1,42)=1.396	0.244
Pain test	Hot plate (latency, sec)		5.959 ± 0.524	6.614 ± 0.347	F(1,42)=1.084	0.3037
Motor tests	Grip strength (*N*)		0.872 ± 0.021	0.908 ± 0.023	F(1,42)=1.337	0.2542
	Wire hang (latency to fall, sec)		49.14 ± 3.861	41.395 ± 4.944	F(1,42)=1.524	0.2238
	Rotarod (latency to fall, sec; average of 6 trials)		123.317 ± 19.859	190.061 ± 20.992	F(1,41)=10.026	0.0029 *
Anxiety-like behavior	Light/dark transition	Distance travelled light (cm)	212.341 ± 36.634	194.718 ± 41.553	F(1,42)=0.101	0.752
		Distance travelled dark (cm)	637.855 ± 72.399	665.655 ± 58.686	F(1,42)=0.089	0.7669
		Stay Time in light (sec)	131.159 ± 29.395	86.773 ± 17.605	F(1,42)=1.678	0.2023
		Transitions (times)	8.5 ± 2.154	8.818 ± 2.1	F(1,42)=0.011	0.9163
		Latency to light (sec)	240.409 ± 50.645	252.182 ± 56.099	F(1,42)=0.024	0.877
	Elevated plus maze	Number of entries (times)	16.045 ± 1.987	10.636 ± 1.482	F(1,42)=4.76	0.0348 *
		Distance travelled (cm)	635.923 ± 42.879	563.991 ± 44.283	F(1,42)=1.362	0.2498
		Entries into open arms (%)	18.815 ± 4.611	14.149 ± 4.227	F(1,42)=0.556	0.4599
		Time on open arms (%)	3.303 ± 0.673	1.557 ± 0.474	F(1,42)=4.492	0.04 *
		Time on closed arms (%)	41.83 ± 5.608	39.951 ± 6.767	F(1,42)=0.046	0.8318
		Time on center arms (%)	54.867 ± 5.391	58.492 ± 6.543	F(1,42)=0.183	0.6711
Depression model	Porsolt forced swim (immobility, %)	Day1	68.960 ± 4.026	76.659 ± 4.304	F(1,42)=5.907	0.0194 *
		Day2	82.703 ± 1.407	90.813 ± 1.086	F(1,42)=8.971	0.0046 *
	Tail suspension (immobility, %)		38.876 ± 2.632	40.365 ± 3.445	F(1,42)=0.065	0.7999
Locomotor activity	Open field	Total distance (cm)	17314.917 ± 1175.132	21645.462 ± 2035.514	F(1,42)=0.262	0.6111
		Vertical activity (times)	1253.25 ± 92.566	1586.846 ± 163.34	F(1,42)=0.881	0.3534
		Center time (sec/min)	8.642 ± 1.329	5.711 ± 0.854	F(1,42)=0.697	0.4084
		Stereotypic count (times)	11198.5 ± 447.585	11506 ± 750.506	F(1,42)=0.532	0.47
Social interaction (one-chamber)	Total duration of contact (sec)		133.545 ± 30.317	222.291 ± 51.266	F(1,20)=2.220	0.1518
	Number of contacts (times)		32.636 ± 5.035	25.455 ± 4.057	F(1,20)=1.234	0.2799
	Total duration of active contacts (sec)		8.764 ± 1.322	5.491 ± 0.836	F(1,20)=4.377	0.0494 *
	Mean duration/Contact		4.136 ± 1.052	19.255 ± 9.236	F(1,20)=2.645	0.1195
	Distance travelled (cm)		2837.818 ± 396.169	2061.455 ± 282.966	F(1,20)=2.543	0.1265
Sensory motor gating	Acoustic startle response	110-dB	0.928 ± 0.187	1.573 ± 0.18	F(1,42)=6.155	0.0172 *
		120-dB	3.593 ± 0.343	3.583 ± 0.349	F(1,42)=0.000381	0.9845
	Prepulse inhibition (startle stimulus, %)	74-110-dB	43.966 ± 7.139	55.17 ± 3.978	F(1,42)=1.869	0.1788
		78-110-dB	48.764 ± 7.537	64.539 ± 4.103	F(1,42)=3.379	0.0731
		74-120-dB	22.549 ± 3.997	21.345 ± 5.031	F(1,42)=0.035	0.8522
		78-120-dB	37.152 ± 4.499	31.314 ± 4.708	F(1,42)=0.804	0.3751
Contextual and cued fear conditioning	Conditioning (freezing, %)		23.190 ± 5.818	27.090 ± 5.388	F(1,42)=1.102	0.2997
	Context (freezing, %)		45.201 ± 6.495	45.349 ± 5.966	F(1,42)=0.001	0.981
	Cue 1-6 min (freezing, %)		61.715 ± 6.158	73.698 ± 5.260	F(1,42)=6.404	0.0152 *
	Cue 1-3 min (freezing, %)		44.468 ± 3.147	60.155 ± 2.970	F(1,42)=6.494	0.0146 *
	Cue 4-6 min (freezing, %)		78.962 ± 4.388	87.241 ± 3.524	F(1,42)=2.958	0.0928

a *<0.05

Behavioral test battery was performed in the following order

General health/neurological screen, wire hang, grip strength test, light/dark transition, open field, elevated plus maze, hot plate, one-chamber social interaction, rotarod, prepulse inhibition, Porsolt forced swim, contextual and cued fear conditioning, three-chamber social interaction test, eight arm radial maze, barnes maze, tail suspension test, 24 hour home cage monitoring.

Table S2

Supplemental Table 2
A list of behavioral tests 129 strain (WT vs matDp/+).

Behavioral test			Mean ± SEM		*F* value	*P* value [a]
			WT	matDp/+		
General health	Weight (g)		24.733 ± 0.539	23.783 ± 0.54	F(1,34)=1.551	0.2215
	Temperature (℃)		37.039 ± 0.125	36.35 ± 0.114	F(1,34)=16.563	0.0003 *
Pain test	Hot plate (latency, sec)		5.9 ± 0.467	6.267 ± 0.588	F(1,34)=0.239	0.6283
Motor tests	Grip strength (*N*)		0.818 ± 0.032	0.803 ± 0.03	F(1,34)=0.118	0.7334
	Wire hang (latency to fall, sec)		57.548 ± 1.555	47.845 ± 4.877	F(1,34)=3.594	0.0665
	Rotarod (latency to fall, sec; average of 6 trials)		165.972 ± 24.433	209.194 ± 20.805	F(1,34)=2.929	0.0961
Anxiety-like behavior	Light/dark transition	Distance travelled light (cm)	458.394 ± 76.262	335.794 ± 60.666	F(1,30)=1.583	0.2181
		Distance travelled dark (cm)	829.781 ± 102.749	683.087 ± 85.098	F(1,30)=1.209	0.2803
		Stay Time in light (sec)	249.094 ± 40.492	163 ± 37.933	F(1,30)=2.408	0.1312
		Transitions (times)	16 ± 3.482	8.125 ± 2.655	F(1,30)=3.234	0.0822
		Latency to light (sec)	137.25 ± 45.996	220.062 ± 57.09	F(1,30)=1.276	0.2676
	Elevated plus maze	Number of entries (times)	20.722 ± 2.825	17.722 ± 2.045	F(1,34)=0.74	0.3957
		Distance travelled (cm)	814.161 ± 71.072	720.333 ± 54.738	F(1,34)=1.094	0.303
		Entries into open arms (%)	20.403 ± 4.16	21.121 ± 4.129	F(1,34)=0.015	0.9033
		Time on open arms (%)	6.389 ± 1.683	4.042 ± 1.168	F(1,34)=1.312	0.26
		Time on closed arms (%)	36.926 ± 5.744	33.19 ± 5.482	F(1,34)=0.221	0.641
		Time on center arms (%)	56.685 ± 5.751	62.769 ± 5.401	F(1,34)=0.595	0.446
Depression model	Porsolt forced swimming (immobility, %)	Day1	55.803 ± 9.307	65.973 ± 12.187	F(1,34)=0.297	0.5896
		Day2	72.002 ± 5.980	73.129 ± 6.512	F(1,34)=0.057	0.8129
	Tail suspension (immobility, %)		39.411 ± 6.613	42.774 ± 7.292	F(1,32)=0.344	0.5619
Locomotor activity	Open field	Total distance (cm)	17314.917 ± 1175.132	21645.462 ± 2035.514	F(1,34)=0.813	0.3737
		Vertical activity (times)	1253.250 ± 92.566	1586.846 ± 163.340	F(1,34)=1.273	0.2671
		Center time (sec/min)	8.642 ± 1.329	5.711 ± 0.854	F(1,34)=1.709	0.1999
		Stereotypic count (times)	11198.500 ± 447.585	11506.000 ± 750.506	F(1,34)=2.579	0.1175
Social interaction (one-chamber)	Total duration of contact (sec)		101.725 ± 26.355	144.978 ± 32.605	F(1,15)=1.030	0.3264
	Number of contacts (times)		34.5 ± 5.134	39.889 ± 5.891	F(1,15)=0.464	0.5061
	Total duration of active contacts (sec)		8.825 ± 1,288	9.111 ± 1.333	F(1,15)=0.024	0.8801
	Mean duration/Contact		2.988 ± 0.441	4.522 ± 1.466	F(1,15)=0.903	0.357
	Distance travelled (cm)		3432.125 ± 412.273	3302.889 ± 388.645	F(1,15)=0.052	0.8226
Sensory motor gating	Acoustic startle response	110-dB	1.023 ± 0.14	2.049 ± 0.448	F(1,34)=4.780	0.0358 *
		120-dB	2.749 ± 0.317	4.668 ± 0.605	F(1,34)=7.900	0.0081 *
	Prepulse inhibition (startle stimulus, %)	74-110-dB	57.249 ± 5.899	41.232 ± 9.067	F(1,34)=2.193	0.1479
		78-110-dB	64.072 ± 6.777	62.357 ± 4.512	F(1,34)=0.044	0.8344
		74-120-dB	19.41 ± 6.097	14.374 ± 4.685	F(1,34)=0.429	0.5169
		78-120-dB	35.054 ± 5.625	23.452 ± 4.944	F(1,34)=2.400	0.1306
Contextual amd cued fear conditioning	Conditioning (freezing, %)		25.290 ± 6.266	25.0674 ± 6.111	F(1,34)=0.002	0.9655
	Context (freezing, %)		47.941 ± 7.304	42.576 ± 6.922	F(1,34)=0.407	0.5279
	Cue 1-6 min (freezing, %)		53.672 ± 8.071	58.410 ± 7.638	F(1,34)=0.822	0.371
	Cue 1-3 min (freezing, %)		27.191 ± 2.816	33.702 ± 2.971	F(1,34)=1.432	0.2396
	Cue 4-6 min (freezing, %)		80.154 ± 5.323	83.119 ± 4.710	F(1,34)=0.211	0.649

a *<0.05